IEEE TRANSACTIONS ON WIRELESS COMMUNICATIONS, VOL. 14, NO. 8, AUGUST 2023 1

A Non-Orthogonal Cross-Tier Joint Transmission Design for Clustered ABS-Assisted Networks

Xianling Wang, *Member, IEEE,* Haijun Zhang, *Fellow, IEEE,* Hongwen Yang, *Member, IEEE,* Yue Tian, *Member, IEEE,* Chen Zhu, and Arumugam Nallanathan, *Fellow, IEEE*

Abstract

Non-orthogonal multiple access (NOMA) has drawn much attention due to its capability in massive connections. It enables various joint designs with advanced technologies, e.g., cooperative transmission and aerial base station (ABS)-assisted networks. In this paper, we consider an efficient NOMA enabled cross-tier joint transmission design. This design jointly applies zero-forcing beamforming and NOMA to realize joint transmission and regular transmission for the users in different tiers. We evaluate the performance of the design under a large-scale clustered ABS-assisted network scenario. Theoretical expressions for the outage probability and area outage spectral efficiency are derived. Numerical results show that, although splitting power may lead to slight degradation for the macro-cell users, the system can still expect a decreased overall outage probability because joint transmission improves the received signal quality for the ABS-tier users. The macro-cell users may not always suffer outage performance degradation since they can keep receiving signals instead of staying idle until the cross-tier joint

X. Wang, Y. Tian and C. Zhu are with Fujian Key Laboratory of Communication Network and Information Processing, Xiamen University of Technology, Xiamen 361024, China (e-mail: xianling.wang@ieee.org; yue.tian.xmut@outlook.com; zhuchen@xmut.edu.cn).

H. Zhang is with Beijing Advanced Innovation Center for Materials Genome Engineering, Beijing Engineering and Technology Research Center for Convergence Networks and Ubiquitous Services, the University of Science and Technology Beijing, Beijing 100083, China (e-mail: haijunzhang@ieee.org).

H. Yang is with Beijing University of Posts and Telecommunications, Beijing 100876, China (e-mail:yanghong@bupt.edu.cn).

A. Nallanathan is with the School of Electronic Engineering and Computer Science, Queen Mary University of London, London E1 4NS, U.K. (e-mail:nallanathan@ieee.org).

Manuscript received XXX; revised XXX.

transmission is suspended as in the orthogonal scheme. Besides, with properly selected NOMA power allocation coefficient, a more reliable communication link can be guaranteed for the macro-cell user, if compared with the conventional orthogonal scheme.

Index Terms

Aerial base station, joint transmission, LoS/NLoS propagation, non-orthogonal multiple access, Poisson cluster process, stochastic geometry, zero-forcing beamforming.

I. Introduction

THE next generation communication system is envisioned to bring in a full-fledged wireless framework, which will support various use cases including autonomous cars, real-time remote surveillance, and disaster relief [1]. To achieve these goals, traditional terrestrial networks are experiencing an integration with various cutting-edge network architectures, such as cell-free networks [2], [3], mobile edge computing [4], [5], and unmanned aerial vehicle (UAV) communication systems [6]. Among them, UAV provides the simplest but also most efficient way to prompt the paradigm shift in network architecture. They can serve as aerial base stations (ABSs), which enable an evolution towards 3D heterogeneous networks (HetNets) for terrestrial cellular infrastructures [7]. Due to their flexible mobility, ABSs can be deployed in unfavourable scenarios, e.g., mountainous terrain and marine area, to guarantee wireless signal coverage at much lower costs [8]. Meanwhile, cooperation can be invoked between macro-cell base stations (MBSs) and ABSs through coordinated multi-point transmission (CoMP) [9]. By means of joint transmission, diversity gain can be obtained, which focuses on improving reliability for user equipments (UEs) at cell-edges.

Although CoMP contributes to coverage improvement, its major drawback can be found in the aspect of spectrum resource utilization. Specifically, in ABS-assisted networks, where accommodating more UEs to achieve multiplexing gain remains a main purpose, each base station (BS) tends to schedule its own UE to maintain a high area spectral efficiency [10]. However, to make good use of joint transmission, CoMP requires additional resources, e.g., BSs and subchannels, for each communication link [11]. Hence implementing CoMP among multiple BSs to serve a mutual UE turns out to be unfavourable for efficiently utilizing BS and spectrum resources.

In orthogonal multiple access (OMA) based systems, diversity and multiplexing can be balanced in a time division multiple access (TDMA) manner, i.e., periodically invoking CoMP for different UEs. Nonetheless, such combination is rather straightforward, leaving much room for developing in-depth integration with higher efficiency and flexibility. Over the past few years, non-orthogonal multiple access (NOMA) has drawn much attention due to its capability in enabling massive connections [12], [13]. In NOMA based systems, each BS can simultaneously transmit signals for multiple UEs on a single time-frequency resource block, which offers a new dimension to facilitate closer combinations for diversity and multiplexing. Given the potential benefits, incorporating CoMP and NOMA in ABS-assisted networks will be with great prospect and investigations on key performance metrics are desirable.

A. Related Works and Motivation

To better exploit high-altitude line-of-sight (LoS) transmission and flexible mobility in ABS-assisted networks, researchers have accomplished numerous studies in the past decade. Recent works include evaluating system performance, as well as adapting resource allocation strategies for ABS-assisted networks. In [10], the authors investigated the system performance of finite ABS-assisted networks with a binomial point process model. They showed that ABS based network densification can achieve higher area spectral efficiency than terrestrial scheme because air-to-ground links experience LoS propagation with higher possibility. In [14], the authors developed a deep reinforcement learning based algorithm, which jointly considered ABS trajectory design and spectrum allocation to realize energy-efficient communication.

Meanwhile, CoMP remains a promising technique in the backdrop of 3D HetNet evolution and continuously gains attention. In CoMP enabled wireless networks, the cooperation between BSs can take different forms, such as interference coordination [15] and physical layer transmission techniques including distributed zero-forcing beamforming (ZF-BF) and non-coherent joint transmission (NC-JT) [16]. Compared with distributed ZF-BF, which heavily relies on sharing channel state information among BSs, NC-JT is more commonly adopted because it takes the advantage of reduced overhead exchange. For terrestrial systems, NC-JT has been applied to realize interference mitigation in user-centric networks [17]. Some researchers also investigated hybrid joint transmission through sub-6 GHz and millimeter wave spectrum [18]. In ABS-assisted networks, the applications of CoMP can also be found. The work in [9] studied cross-tier joint transmission among ABS and ground BSs for cell-edge UEs in emergency communication

scenarios. The work in [19] proposed coordinating ABS interference through NC-JT, where user-centric cooperating ABSs were organized according to signal strength. These works have built up effective approaches to fundamentally study CoMP in ABS-assisted networks.

In addition, great progress can be witnessed in the integration of NOMA and various physical layer technologies, such as simultaneous wireless information and power transfer [20], coordinated relay network [21], cognitive radio network [22], and Terahertz communications [23]. Studies have also been carried out to reap the benefit of NOMA for CoMP systems and ABS-assisted networks. In [24], the authors proposed a NOMA enabled downlink joint transmission framework, where each BS can superimpose the cooperating signal of a cell-edge UE with that of another cell-center UE. This framework preliminarily explored balancing diversity and multiplexing through NOMA for CoMP systems. In [25], NOMA was introduced into a multi-ABS aided joint transmission network to improve system sum rate. The work in [26] presented a multiple-input multiple-output (MIMO) NOMA design for ABS-assisted networks. A signal alignment strategy was proposed to realize block diagonalization based BF for NOMA users. The work in [27] addressed energy efficiency optimization problem for NOMA downlink communication in ABS-assisted networks.

Inspired by the potential profit illustrated in [24], [25], we consider a NOMA enabled cross-tier joint transmission framework for clustered ABS-assisted networks in this paper. To the best of our knowledge, few effort has been put in this context, and the benefit of supporting reliable transmission without interrupting massive connections is not yet identified. Though the authors in [9] similarly considered cross-tier joint transmission in ABS-assisted networks, their work was focused on OMA based user-centric systems, which neglected the capability of NOMA in improving sum rate performance. Another related work in [24] explored the joint design of NOMA and CoMP, but the practical clustering and hierarchical relationship between different BS tiers were not taken into consideration. Part of the study was published in [28], and this paper extends [28] in following ways: 1) The 2D terrestrial scenario is extended into 3D non-terrestrial scenario, where network densification relies on ABSs. 2) The topology is extended from single cell to multiple cells, leading to higher complexity in the theoretical analysis. 3) Enriched results are provided to study the impacts of system parameters.

B. Contributions

The main contributions of the paper are summarized as follows.

1) Integrating NOMA with Cross-Tier Joint Transmission: We consider an efficient ZF-BF-NOMA enabled cross-tier joint transmission design. The basic idea of this design is to jointly apply ZF-BF and NOMA for an MBS to provide multiple two-user NOMA streams, where the two NOMA UEs are in different tiers. Upon this design, a UE in the ABS-tier can receive signal from an MBS and an ABS at the same time to achieve diversity, while a UE in the MBS-tier can keep receiving its desired signal instead of staying idle until the joint transmission is suspended. This design provides additional communication link through NOMA, thus realizing joint transmission in a more efficient way while keeping the original purpose of network densification.

2) Modeling and Performance Evaluation under Clustered ABS-Assisted Networks: We develop an analytical framework to evaluate the system performance of ZF-BF-NOMA enabled cross-tier joint transmission under clustered network topology. To be specific, we assume a Poisson cluster process based random network, where each MBS deploys multiple ABSs in its coverage area. Such assumption is more in line with practical clustering and hierarchical relationship between BSs in different tiers. Under probabilistic LoS propagation model, we resort to stochastic geometry to deal with aggregate interference, and provide theoretical outage probability and area outage spectral efficiency of the system.

3) System Design Guidelines: We study the impacts of different parameters including ABS height, ABS number, and antenna number based on the developed analytical framework. We also compare the NOMA based joint transmission and the traditional OMA based one, and show that NOMA is superior to OMA under a wide range of practical system setup. Moreover, we theoretically provide the sufficient condition on NOMA power allocation coefficient to wipe out the negative effect of splitting the transmit power for the UEs in the MBS-tier.

The rest of the paper is organized as follows. In Section II, we describe the considered clustered ABS-assisted network model, as well as the NOMA enabled cross-tier CoMP transmission. In Section III, we firstly provide some preliminary results regarding distance distributions and then analyze the statistical characteristics for the desired signal and interfering signal. In Section IV, we derive outage probabilities and area outage spectral efficiency. Section V validates our theoretical outage probability expressions and provides discussions on the observations obtained through numerical calculation. Finally, conclusions are drawn in Section VI.

II. System Model

A. Network Model

We consider a downlink two-tier HetNet, where MBSs and ABSs coexist in the system. Assume that each MBS is with height h_{M}, and the set of all MBSs forms a Poisson point process (PPP) with density λ_{M} denoted by $\Omega = \{\mathbf{b}_i \in \mathbb{R}^2_{\mathrm{M}}, i \in \mathbb{N}\}$, where $\mathbf{b}_i$ represents the i-th MBS in Ω, and $\mathbb{R}^2_{\mathrm{M}}$ is a 2D plane parallel to the ground $\mathbb{R}^2_{\mathrm{U}}$ with distance h_{M}. With a slight abuse of notation, we also use $\mathbf{b}_i$ to represent the i-th MBS's coordinate.[1] Let $\mathbf{b}'_i$ be the projection of $\mathbf{b}_i$ on $\mathbb{R}^2_{\mathrm{U}}$. For network densification, each MBS deploys N_{s} ABSs with height $h_{\mathrm{A}} > h_{\mathrm{M}}$ in its coverage area, forming ABS clusters. Note that we consider fixed and identical ABS height, since our focus is on transmission strategy. Assuming varying ABS height will reduce tractability but hardly reveal important guidance on designing transmission strategy. In addition, neglecting small variation in ABS height will only cause slight accuracy loss as presented in [10]. For better illustration, an example of the clustered two-tier network is shown in Fig. 1a. Denote by $\Psi_i = \{\mathbf{d}_{i,n} \in \mathbb{R}^2_{\mathrm{A}}, n = 1 : N_{\mathrm{s}}\}$ the ABS cluster attached to $\mathbf{b}_i$, where $\mathbf{d}_{i,n}$ represents the n-th ABS in Ψ_i, and $\mathbb{R}^2_{\mathrm{A}}$ is a 2D plane parallel to $\mathbb{R}^2_{\mathrm{U}}$ with distance h_{A}. Let $\Psi = \cup_{\mathbf{b}_i \in \Omega} \Psi_i$ be the set of all ABSs, $\Phi_i = \{\mathbf{b}_i\} \cup \Psi_i$ be the set of $\mathbf{b}_i$ and all of its attached ABSs, and $\Phi = \Omega \cup \Psi$ be the set of all MBSs and ABSs. By definition, Φ is a Poisson cluster process (PCP), with Ω and Ψ being the parent point process and offspring point process[2], respectively [29].

To evaluate system performance, we randomly choose a *representative MBS* and denote it by $\mathbf{b}_0$. Hence, the set of the representative MBS and its attached ABSs can be denoted by Φ_0, which is termed *representative cluster*. Let $\mathbf{b}'_0$ be the origin of the 3D coordinate, and $\Omega_+ = \{\mathbf{b}_i, i \in \mathbb{N}^+\}$ be the set of all MBSs excluding $\mathbf{b}_0$. So we have $\Psi_+ = \cup_{\mathbf{b}_i \in \Omega_+} \{\mathbf{d}_{i,n}, n = 1 : N_{\mathrm{s}}\}$ and $\Phi_+ = \Omega_+ \cup \Psi_+$.

We specialize Φ to Matérn cluster process (MCP). To be specific, for $\mathbf{b}_i$, its N_{s} attached ABSs are uniformly and identically distributed in a circular area $\mathcal{B}''_i = \mathcal{B}(\mathbf{b}''_i, r_{\mathrm{s}})$ in $\mathbb{R}^2_{\mathrm{A}}$, where $\mathcal{B}(\mathbf{b}''_i, r_{\mathrm{s}})$ represents a 2D disk centered at $\mathbf{b}''_i$ with radius r_{s} parallel to $\mathbb{R}^2_{\mathrm{U}}$, and $\mathbf{b}''_i$ is the projection of $\mathbf{b}_i$ on $\mathbb{R}^2_{\mathrm{A}}$. Denote by $D_{i,n}$ the distance from $\mathbf{b}_i$ to $\mathbf{d}_{i,n}$. An example of the nodes

[1]This slight notational abuse also applies for other nodes in the following.

[2]The considered PCP is a simplified one as the offspring points in each cluster are deterministic in number.

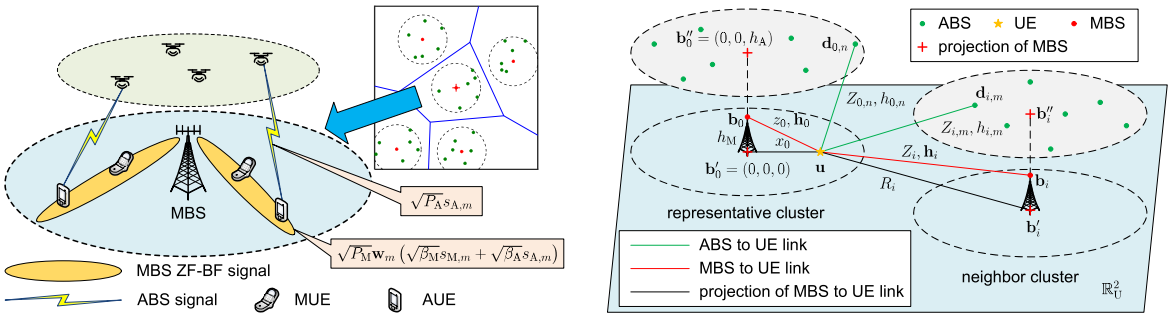

(a) Scenario and transmission process: 1) Each ABS directly transmits to its active AUE, while each MBS applies ZF-BF and transmits superimposed signal to an AUE and an MUE in each stream. 2) Each MUE only receives signal from its associated MBS, while an AUE can receive enhanced signal through cross-tier NC-JT.

(b) Distance and small-scale fading: 1) $\mathbf{u}$ is located at $(x_0,0,0)$ in $\mathbb{R}^2_{\rm U}$, while all ABSs hover in $\mathbb{R}^2_{\rm A}$. 2) Z_i and $Z_{i,m}$ represents the distance from $\mathbf{b}_i$ and $\mathbf{d}_{i,m}$ to $\mathbf{u}$, respectively, while $\mathbf{h}_i$ and $h_{i,m}$ are the corresponding small-scale fading amplitude gains.

Fig. 1. MCP based ABS-assisted network scenario, transmission process, and distance illustrations.

can be found in Fig. 1b. By definition, the probability density function (PDF) of $D_{i,n}$ is

$$f_{D_{i,n}}(d)=\begin{cases}\dfrac{2d}{r_{\rm s}^2}, & 0\le d\le r_{\rm s},\\ 0, & \text{otherwise.}\end{cases} \tag{1}$$

We consider clustered UE distribution, where UEs are randomly distributed around each MBS. Specifically, for $\mathbf{b}_i$, assume that its serving UEs are uniformly and identically distributed in a circular area $\mathcal{B}_i'=\mathcal{B}(\mathbf{b}_i',r_{\rm s})$ in $\mathbb{R}^2_{\rm U}$. To facilitate analysis, we arbitrarily choose a UE served by $\mathbf{b}_0$ and denote it by $\mathbf{u}$. This UE is referred to as *typical UE*. We align the x-axis of the coordinate with $\mathbf{u}$ due to the rotational invariant of PCP. Denote by R_i and $R_{i,n}$ the horizontal distance from $\mathbf{b}_i$ and $\mathbf{d}_{i,n}$ to $\mathbf{u}$, respectively. Let $Z_i=\sqrt{R_i^2+h_{\rm M}^2}$ and $Z_{i,n}=\sqrt{R_{i,n}^2+h_{\rm A}^2}$ be the Euclidean distance from $\mathbf{b}_i$ and $\mathbf{d}_{i,n}$ to $\mathbf{u}$, respectively. Assuming that the distance from $\mathbf{u}$ to $\mathbf{b}_0'$ is $R_0=x_0$ with PDF calculated by (1) as $f_{R_0}(x_0)=f_{D_{i,n}}(x_0)$, we have $z_0=\sqrt{x_0^2+h_{\rm M}^2}$ being the distance from $\mathbf{b}_0$ to $\mathbf{u}$. See Fig. 1b for detailed distance illustration.

B. Channel Model

Assume that the MBS-tier and ABS-tier both operate in sub-6 GHz spectrum. Each MBS is equipped with M ($M\le N_{\rm s}$) antennas and transmits with total power $P_{\rm M}$. All ABSs and UEs are equipped with single antenna, and the transmit power of each ABS is $P_{\rm A}$.

Consider composite power-law path-loss and frequency non-selective small-scale fading signal propagation model. The signal amplitude gain of the $\mathbf{b}_i$–$\mathbf{u}$ link can be expressed as $\sqrt{Z_i^{-\alpha}}\mathbf{h}_i$, where row vector $\mathbf{h}_i \in \mathbb{C}^{1\times M}$ is the small-scale fading amplitude gain from $\mathbf{b}_i$ to $\mathbf{u}$, and α is path-loss exponent. Likewise, the signal amplitude gain of the $\mathbf{d}_{i,n}$–$\mathbf{u}$ link is $\sqrt{Z_{i,n}^{-\alpha}}h_{i,n}$, where scalar $h_{i,n}$ is the small-scale fading amplitude gain. We consider probabilistic LoS and non-line-of-sight (NLoS) propagation for air-to-ground channel and distinguish α as α_{L} and α_{N} ($2 < \alpha_{\mathrm{L}} < \alpha_{\mathrm{N}}$) for LoS and NLoS link, respectively. As for ground-to-ground channel, we assume deterministic NLoS propagation, i.e., $\alpha = \alpha_{\mathrm{N}}$ for the $\mathbf{b}_i$–$\mathbf{u}$ link, because MBS is much lower than ABS and blockage occurs with much higher likelihood. Assuming Nakagami-m fading channel, the small-scale fading power gain obeys $\mathrm{Gamma}\left(m_k, 1/m_k\right)$, where $\mathrm{Gamma}(a,b)$ represents Gamma distribution with shape parameter a and scale parameter b, m_k is the integer Nakagami-m parameter, and $k \in \{\mathrm{L},\mathrm{N}\}$ for LoS and NLoS.

According to [30], the occurrence probability $p_{\mathrm{L}}\left(\phi_{i,n}\right)$ of LoS $\mathbf{d}_{i,n}$–$\mathbf{u}$ link is determined by the elevation angle $\phi_{i,n}$ from $\mathbf{d}_{i,n}$ to $\mathbf{u}$. Given fixed ABS height, $\phi_{i,n}$ is calculated solely on $Z_{i,n}$, so the LoS and NLoS probabilities are rewritten as

$$p_{\mathrm{L}}(Z_{i,n}) = \frac{1}{1 + c\exp\left(-b\left(\arcsin\left(\frac{h_{\mathrm{A}}}{Z_{i,n}}\right) - c\right)\right)}, \tag{2}$$

and $p_{\mathrm{N}}(Z_{i,n}) = 1 - p_{\mathrm{L}}(Z_{i,n})$, where b and c are constant parameters depending on environments, and $\arcsin\left(\frac{h_{\mathrm{A}}}{Z_{i,n}}\right)$ calculates the elevation angle in degree.

For brevity, the LoS ABS and NLoS ABS is termed LBS and NBS, respectively, and $\mathbf{d}_{i,n}$ is divided into $\bar{\mathbf{d}}_{i,n}$ and $\hat{\mathbf{d}}_{i,n}$ accordingly. Note that other corresponding distances and small-scale fading gains are also marked as "$\bar{X}$" and "$\hat{X}$" to distinguish LoS and NLoS. The prefix of "L" and "N" is also frequently used to distinguish the LoS and NLoS state for BSs and UEs as well.

C. Association Policy

In practical systems, a UE in downlink transmission generally maintains a data channel and a control channel with the network, e.g., physical downlink shared channel (PDSCH) and physical downlink control channel (PDCCH) in long term evolution (LTE). Since the equipment mounted by an ABS is usually simplified with partial functions, we assume that MBSs can manage both data and control channel, while ABSs are only capable of transmitting data traffics. Meanwhile, given the hierarchical relationship between an MBS and its attached ABSs, we also assume that a UE receives control signals from an MBS and receives data traffics from either the same MBS

or one of its attached ABSs. We consider closed access policy. Hence, $\mathbf{u}$ is prohibited from receiving control signals from any $\mathbf{b}_i$ other than $\mathbf{b}_0$, even though $\mathbf{b}_i$ may be closer than $\mathbf{b}_0$.

Our evaluation focuses on data channel because control channel normally occupies dedicated spectrum and is much more reliable. Therefore, following description and analysis are all upon data channel and related cumbersome explanations are omitted hereafter. Assume biased maximum received signal strength indicator (RSSI) based association policy within a cluster. To be specific, $\mathbf{u}$ will be associated with $\mathbf{b}_0$ and become an MBS UE (MUE) if $P_{\mathrm{A}} Z_{0,\star}^{-\alpha} < \frac{P_{\mathrm{M}}}{M} B z_0^{-\alpha_{\mathrm{N}}}$, where P_{M} is equally divided for M streams, and $Z_{0,\star}$ is the distance from the strongest ABS in the cluster indicated by $\mathbf{d}_{0,\star}$ to $\mathbf{u}$. Likewise, $\mathbf{d}_{0,\star}$ differs as $\bar{\mathbf{d}}_{0,\star}$ and $\hat{\mathbf{d}}_{0,\star}$ for the strongest LBS and NBS. If $P_{\mathrm{A}} Z_{0,\star}^{-\alpha} \geq \frac{P_{\mathrm{M}}}{M} B z_0^{-\alpha_{\mathrm{N}}}$, $\mathbf{u}$ will be associated with $\mathbf{d}_{0,\star}$ and become an ABS UE (AUE), which will be further labeled as LBS AUE (LUE) and NBS AUE (NUE) depending on whether $\bar{\mathbf{d}}_{0,\star}$ or $\hat{\mathbf{d}}_{0,\star}$ is providing the strongest received signal power. Note that $0 < B \leq 1$ is a traffic offloading bias encouraging UEs to retrieve data traffics from the ABSs.

D. ZF-BF-NOMA Enabled Cross-Tier Joint Transmission

With M antennas, an MBS can apply ZF-BF to maintain M parallel data streams, while an ABS can only provide one stream with its single antenna. Although a BS can be connected with several UEs, not all UEs are scheduled at a time due to the limit of available streams. At any moment, an MBS and an ABS schedules M MUEs and one AUE, respectively, which we term *active MUEs* and *active AUE*. Other connected UEs of a BS are scheduled in a round robin manner. So we have M active MUEs and N_{s} active AUEs in a cluster at the same time.

We introduce cross-tier joint transmission for AUEs. In this strategy, each MBS not only provides desired signals to its active MUEs, but is also coordinated to jointly transmit with its attached ABSs. Given limited resource, an MBS applies power-domain NOMA in each stream and superimposes the signals of an active MUE and an active AUE with power allocation coefficient β_{M} and $\beta_{\mathrm{A}} = 1 - \beta_{\mathrm{M}}$ as shown in Fig. 1a. Since MUEs normally locate closer than AUEs to the MBS, we set $\beta_{\mathrm{A}} > \beta_{\mathrm{M}}$ to guarantee fairness according to the common principle of NOMA that more power should be allocated to the UE with poorer channel condition[3]. The two UEs are selected under following rule, which takes the representative cluster as an example:

[3]In fact, the AUE does not need to be experiencing poorer channel condition than its pairing MUE in this framework. Because the main purpose of setting $\beta_{\mathrm{A}} > \beta_{\mathrm{M}}$ also lies in guaranteeing signal quality enhancement at the AUE and consistent decoding order for the same type of UEs.

1) Firstly, $\mathbf{b}_0$ picks M ABSs among its N_s attached ABSs in a round robin manner, constituting set $\{\mathbf{r}_{0,m}, m = 1 : M\}$, where $\mathbf{r}_{0,m}$ represents a selected ABS.
2) Then, for the m-th stream, $\mathbf{b}_0$ chooses an MUE located at the same direction with the active AUE of $\mathbf{r}_{0,m}$ to form the UE pair for NOMA.

We assume that each MBS is almost sure to find a pairing MUE for each stream, because in hotspot scenarios UEs are densely distributed in all directions[4]. Though, the modeling of direction misalignment can be an interesting extension and will be studied in the future. Let $\mathbf{w}_m$ be the BF vector for the m-th stream of $\mathbf{b}_0$. In ZF-BF transmission, $\mathbf{w}_m$ is generated by the concatenated matrix of M channel direction vectors. Since the paired UEs are at the same direction, they can share the same $\mathbf{w}_m$ to eliminate inter-stream interference simultaneously [31]. To sum up, in the representative cluster, we have that: 1) $\mathbf{b}_0$ transmits the signals of M active MUEs and M active AUEs in M parallel streams. 2) N_s ABSs transmit signals for N_s active AUEs, respectively, at the same time. 3) M out of N_s active AUEs are receiving enhanced signals from MBS and ABS, termed *enhanced AUEs*; $N_\mathrm{s} - M$ out of N_s active AUEs are receiving unenhanced signals solely from ABS, termed *regular AUEs*.

Then we describe the process for signal reception. For an active MUE, it receives the interfering signal of its pairing AUE, which is stronger than its desired signal due to joint transmission and $\beta_\mathrm{A} > \beta_\mathrm{M}$. Therefore, each MUE applies successive interference cancellation (SIC) to remove the signal of its pairing AUE before decoding its desired signal. We consider imperfect SIC that μ of the total NOMA interference power will be remaining after the SIC. Regarding the AUE, it will receive an enhanced signal if this AUE is selected by the MBS in the ZF-BF-NOMA transmission[5]. Otherwise, it solely receives unenhanced signal from its associated ABS. For both cases, the desired signal will be predominating in the received signal. Hence, each active AUE, either regular or enhanced, can directly decode its desired signal without SIC.

[4]In practical system, the MBS may not always be able to find an MUE at the same direction with the active AUE. In this case, the MBS can temporarily suspend NOMA to serve only one UE in that stream, and the system degrades to the benchmark OMA based joint transmission for that moment, which will be discussed in Section II-E.

[5]According to [32], by carefully designing the cyclic delay length of each BS, a coherent power combination can be achieved at the UE.

E. Benchmark OMA Based Joint Transmission

We choose an OMA based joint transmission strategy for comparison. In this benchmark strategy, time is slotted and split into odd and even slots. Each MBS transmits the signals for its M active MUEs using all M streams in the odd slots, while the even slots are reserved for the M enhanced AUEs. For ABSs, they use both odd and even slots to serve their active AUEs. By comparing with NOMA based strategy, we conclude the resource utilization in OMA based strategy that: 1) Each active MUE only has half of the time resources, i.e., odd slots, compared with NOMA based strategy. 2) Each regular active AUE receives unenhanced signal solely from its associated ABS in all time slots. 3) Each enhanced active AUE periodically receives enhanced signal in the even slots, and unenhanced signal in the odd slots.

F. Performance Metrics

We focus on evaluating the outage probability of the active UE and the area outage spectral efficiency (ASE) of the system. The outage probability measures the occurrence probability that the experienced spectral efficiency (SE) of an active UE is lower than a predefined threshold ς. This target SE can be converted into target signal-to-interference ratio (SIR) according to Shannon's formula. Thus, the outage probability for the typical UE can be formally calculated as $\mathcal{O}_k^y = \mathbb{P}\left(\gamma_k^y < \epsilon_k^y\right)$, which is the cumulative distribution function (CDF) of the SIR. Note that γ_k^y and ϵ_k^y represents the SIR and its target value, respectively, where $k \in \{\mathrm{M}, \mathrm{A}, \mathrm{L}, \mathrm{N}, \mathrm{RL}, \mathrm{RN}, \mathrm{EL}, \mathrm{EN}\}$ indicates MUE, AUE, LUE, NUE, regular LUE, regular NUE, enhanced LUE, and enhanced NUE, and $y \in \{\mathrm{NC}, \mathrm{OC}, \text{OC-M}, \text{OC-A}\}$ indicates NOMA based CoMP, OMA based CoMP, and the odd and even slots in OMA based CoMP.

Based on previous discussion, we now express the SIR for the MUE under NC as

$$\gamma_{\mathrm{M}}^{\mathrm{NC}} = \frac{\frac{P_{\mathrm{M}}\beta_{\mathrm{M}}|\mathbf{h}_0\mathbf{w}_m|^2}{z_0^{\alpha_{\mathrm{N}}}}}{\frac{\mu P_{\mathrm{M}}\beta_{\mathrm{A}}|\mathbf{h}_0\mathbf{w}_m|^2}{z_0^{\alpha_{\mathrm{N}}}} + \sum_{n=1}^{N_{\mathrm{s}}-1}\frac{P_{\mathrm{A}}h_{0,n}^2}{Z_{0,n}^{\alpha}} + \sum_{\mathbf{b}_i\in\Omega_+}\left(\sum_{m=1}^{M}\frac{P_{\mathrm{M}}|\mathbf{h}_i\mathbf{w}_{i,m}|^2}{Z_i^{\alpha_{\mathrm{N}}}} + \sum_{\mathbf{d}_{i,n}\in\Psi_i}\frac{P_{\mathrm{A}}h_{i,n}^2}{Z_{i,n}^{\alpha}}\right)}, \tag{3}$$

where $\mathbf{w}_{i,m}$ represents the BF vector for the m-th stream of $\mathbf{b}_i$, $N_{\mathrm{s}}-1$ ABSs contribute to the interference in Ψ_0 due to the effect of imperfect SIC over the signal for the AUE in the NOMA pair. Let $I_{\mathbf{b}_0} = V_1 = \frac{P_{\mathrm{M}}|\mathbf{h}_0\mathbf{w}_m|^2}{z_0^{\alpha_{\mathrm{N}}}}$, $V_2 = \frac{P_{\mathrm{A}}h_{0,\star}^2}{Z_{0,\star}^{\alpha}}$, $I_{\Psi_0} = \sum_{\mathbf{d}_{0,n}\in\Psi_0}\frac{P_{\mathrm{A}}h_{0,n}^2}{Z_{0,n}^{\alpha}}$, $I_{\Psi_\star} = \sum_{\mathbf{d}_{0,n}\in\Psi_0\setminus\mathbf{d}_{0,\star}}\frac{P_{\mathrm{A}}h_{0,n}^2}{Z_{0,n}^{\alpha}}$, $I_{\Psi_+} = \sum_{\mathbf{d}_{i,n}\in\Psi_+}\frac{P_{\mathrm{A}}h_{i,n}^2}{Z_{i,n}^{\alpha}}$, $I_{\Omega_+} = \sum_{\mathbf{b}_i\in\Omega_+}\sum_{m=1}^{M}\frac{P_{\mathrm{M}}|\mathbf{h}_i\mathbf{w}_{i,m}|^2}{Z_i^{\alpha_{\mathrm{N}}}}$. The SIRs for other cases can be expressed as

$$\gamma_{\mathrm{EA}}^{\mathrm{NC}} = \frac{\beta_{\mathrm{A}}V_1 + V_2}{\beta_{\mathrm{M}}I_{\mathbf{b}_0} + I_{\Psi_\star} + I_{\Omega_+} + I_{\Psi_+}}, \quad \gamma_{\mathrm{RA}}^{\mathrm{NC}} = \gamma_{\mathrm{EA}}^{\text{OC-M}} = \gamma_{\mathrm{RA}}^{\mathrm{OC}} = \frac{V_2}{I_{\mathbf{b}_0} + I_{\Psi_\star} + I_{\Omega_+} + I_{\Psi_+}},$$

$$\gamma_{\mathrm{M}}^{\mathrm{OC}} = \frac{V_1}{I_{\Psi_0} + I_{\Omega_+} + I_{\Psi_+}}, \quad \gamma_{\mathrm{EA}}^{\mathrm{OC\text{-}A}} = \frac{V_1 + V_2}{I_{\Psi_\star} + I_{\Omega_+} + I_{\Psi_+}}. \tag{4}$$

The other interested metric is the ASE, which is defined as the achievable SE of a unit area given target user SE threshold. This metric is calculated based on outage probability. For readers' convenience, the expression will be formally given after deriving the outage probability.

III. Distance and Signal Power Distributions

In general, the CDF of the SIR involves the statistical characteristics of distances given different UE associations, which can be seen in (3) and (4). Relevant results have been readily obtained in previous work so we directly provide them in the following Lemma 1 to 4.

A. Preliminary Results

We start from the PDF of $Z_{i,n}$, which is the distance between $\mathbf{u}$ and an arbitrary ABS, i.e., $\mathbf{d}_{i,n}$, in any cluster. This PDF is conditioned on the horizontal distance from $\mathbf{b}_i$ to $\mathbf{u}$, and is given in Lemma 1.

Lemma 1 (Distribution of distance from ABS in any cluster to typical UE): The PDF of $Z_{i,n}$ conditioned on $R_i = r_i$ is expressed as (5) and (6) for $r_i \leq r_{\mathrm{s}}$ and $r_i > r_{\mathrm{s}}$, respectively, that

$$f_{Z_{i,n}}(z|r_i) = \begin{cases} \dfrac{2z}{r_{\mathrm{s}}^2}, & z_{\mathrm{l}} \leq z \leq z_{\mathrm{m}}, \\ \dfrac{2z}{\pi r_{\mathrm{s}}^2} \arccos\left(\dfrac{z^2 - h_{\mathrm{A}}^2 + r_i^2 - r_{\mathrm{s}}^2}{2r_i\sqrt{z^2 - h_{\mathrm{A}}^2}}\right), & z_{\mathrm{m}} < z \leq z_{\mathrm{u}}, \\ 0, & \text{otherwise}, \end{cases} \tag{5}$$

and

$$f_{Z_{i,n}}(z|r_i) = \begin{cases} \dfrac{2z}{\pi r_{\mathrm{s}}^2} \arccos\left(\dfrac{z^2 - h_{\mathrm{A}}^2 + r_i^2 - r_{\mathrm{s}}^2}{2r_i\sqrt{z^2 - h_{\mathrm{A}}^2}}\right), & z_{\mathrm{m}} \leq z \leq z_{\mathrm{u}}, \\ 0, & \text{otherwise}, \end{cases} \tag{6}$$

where $z_{\mathrm{m}} = \sqrt{h_{\mathrm{A}}^2 + (r_s - r_i)^2}$, $z_{\mathrm{u}} = \sqrt{h_{\mathrm{A}}^2 + (r_s + r_i)^2}$, and $z_{\mathrm{l}} = h_{\mathrm{A}}$.

Note that, by setting $R_i = x_0$, $f_{Z_{i,n}}(z|r_i)$ degrades to the PDF of $Z_{0,n}$, which is the distance between $\mathbf{u}$ and an arbitrary ABS, i.e., $\mathbf{d}_{0,n}$, in the representative cluster. Thus, the PDF of $Z_{0,n}$ conditioned on $R_0 = x_0$ can be calculated by (5) as $f_{Z_{0,n}}(z|x_0)$, where $x_0 < r_{\mathrm{s}}$ because $\mathbf{u}$ is distributed in $\mathcal{B}(\mathbf{b}_0', r_{\mathrm{s}})$.

Secondly, we provide in Lemma 2 the association probability. For conciseness, the conditional PDF of $Z_{i,n}$ is rewritten as $f_{Z_{i,n}}(z)$ hereafter.

Lemma 2 (Association probability): The probability that $\mathbf{u}$ at $(x_0, 0, 0)$ is associated with $\bar{\mathbf{d}}_{0,\star}$ and $\hat{\mathbf{d}}_{0,\star}$ can be calculated by a unified expression in (7), given by

$$\mathcal{A}_k = N_{\mathrm{s}} \int_{z_{\mathrm{l}}}^{w_k} B_k(w) p_k(w) f_{Z_{0,n}}(w) \mathrm{d}w, \quad k \in \{\mathrm{L}, \mathrm{N}\}, \tag{7}$$

where $w_k = \min\left\{ \left(\frac{MP_{\mathrm{A}}}{BP_{\mathrm{M}}}\right)^{\frac{1}{\alpha_k}} z_0^{\frac{\alpha_{\mathrm{N}}}{\alpha_k}}, z_{\mathrm{u}} \right\}$,

$$B_k(w) = \left(\sum_{\nu \in \{\mathrm{L},\mathrm{N}\}} \int_{d_{k,\nu}(w)}^{z_{\mathrm{u}}} f_{Z_{0,n}}(u) p_k(u) \mathrm{d}u \right)^{N_{\mathrm{s}}-1}, \tag{8}$$

and $d_{k,\nu}(w) = \min\left\{ w^{\frac{\alpha_k}{\alpha_\nu}}, z_{\mathrm{u}} \right\}$. The probability that $\mathbf{u}$ is associated with $\mathbf{b}_0$ can be calculated as

$$\mathcal{A}_{\mathrm{M}} = \left(\sum_{\nu \in \{\mathrm{L},\mathrm{N}\}} \int_{w_\nu}^{z_{\mathrm{u}}} f_{Z_{0,n}}(u) p_\nu(u) \mathrm{d}u \right)^{N_{\mathrm{s}}}. \tag{9}$$

The other two conditional distance distributions are given in Lemma 3 and 4, respectively.

Lemma 3 (Serving link distance distribution): Given $\mathbf{u}$ at $(x_0, 0, 0)$ being an AUE, the conditional PDF $f_{Z_{0,\star}|k}(z)$ ($k \in \{\mathrm{L}, \mathrm{N}\}$) of the distance $Z_{0,\star}$ from $\mathbf{u}$ to its serving ABS is

$$f_{Z_{0,\star}|k}(z) = \frac{N_{\mathrm{s}}}{\mathcal{A}_k} B_k(z) p_k(z) f_{Z_{0,n}}(z), \quad z_{\mathrm{l}} \le z \le w_k. \tag{10}$$

Lemma 4 (Intra-cluster interfering link distance distribution): Let $\mathcal{E}_{\mathrm{L}}$ and $\mathcal{E}_{\mathrm{N}}$ indicate the event that "$\mathbf{d}_{0,n}$ is a LBS" and "$\mathbf{d}_{0,n}$ is a NBS", respectively. Given $\mathcal{E}_\delta$ ($\delta \in \{\mathrm{L}, \mathrm{N}\}$) with nearest distance d_δ constraint, the conditional PDF $f_{Z_{0,n}|\mathcal{E}_\delta}(z|d_\delta)$ of the distance $Z_{0,n}$ is

$$f_{Z_{0,n}|\mathcal{E}_\delta}(z|d_\delta) = \frac{f_{Z_{0,n}}(z) p_\delta(z)}{\int_{d_\delta}^{z_{\mathrm{u}}} f_{Z_{0,n}}(u) p_\delta(u) \mathrm{d}u}, \quad d_\delta \le z \le z_{\mathrm{u}}. \tag{11}$$

Detailed proof for above Lemma 1 to 4 can be found in [10] and is omitted due to space limit.

B. Combined Signal Power Distribution

It can be seen in the SIR expressions that the desired signal power involves random variable (RV) $V_1 = \frac{P_{\mathrm{M}}|\mathbf{h}_0 \mathbf{w}_m|^2}{z_0^{\alpha_{\mathrm{N}}}}$ and $V_2 = \frac{P_{\mathrm{A}} h_{0,\star}^2}{Z_{0,\star}^{\alpha}}$, as well as their weighted sums, i.e., $\beta_{\mathrm{A}} V_1 + V_2$ and $V_1 + V_2$. For convenience, we unify these two expressions as $V = a_1 V_1 + a_2 V_2$, where $a_1 = \beta_{\mathrm{A}}$, $a_2 = 1$ for $\gamma_{\mathrm{EA}}^{\mathrm{NC}}$ and $a_1 = a_2 = 1$ for $\gamma_{\mathrm{EA}}^{\mathrm{OC\text{-}A}}$. The CDF of V_1, V_2, and V are provided in Lemma 5.

Lemma 5 (Desired signal power distribution): The desired signal power V_i ($i \in \{1,2\}$) follows Gamma distribution with shape parameter m_i and scale parameter θ_i, and the CDF is given by

$$F_{V_i}(v) = \texttt{GamCDF}(v, m_i, \theta_i), \qquad m_1 = m_{\mathrm{N}}, \quad \theta_1 = \frac{P_{\mathrm{M}} z_0^{-\alpha_{\mathrm{N}}}}{M m_{\mathrm{N}}}, \\ m_2 = m_k, \quad \theta_2 = \frac{P_{\mathrm{A}} Z_{0,\star}^{-\alpha_k}}{m_k}, \quad k \in \{\mathrm{L}, \mathrm{N}\}, \tag{12}$$

where $\texttt{GamCDF}(v, m, \theta)$ represents the CDF of Gamma distributed RV with shape parameter m and scale parameter θ. The CDF of $V = a_1 V_1 + a_2 V_2$ can be expressed as (13), given by

$$F_V(v) = \sum_{i=1}^{2} \sum_{j=1}^{m_i} c_{i,j} \left(-a_i \theta_i\right)^j \texttt{GamCDF}\left(v, j, a_i \theta_i\right), \tag{13}$$

$$c_{i,j} = \left(-\frac{1}{a_i \theta_i}\right)^{m_i} \binom{m_{3-i} + m_i - j - 1}{m_i - j} \frac{\left(a_{3-i}\theta_{3-i}\right)^{m_i - j}}{\left(1 - \frac{a_{3-i}\theta_{3-i}}{a_i \theta_i}\right)^{m_{3-i} + m_i - j}}. \tag{14}$$

Note that m_2 and θ_2 take different values for LUE and NUE, respectively.

Proof: See Appendix A. ■

It can be observed in (13) that exact statistical study on the combined signal power requires the summation of the CDFs of multiple Gamma distributed RVs. Such summation will increase complexity during numerical calculation. So we approximate the results in Corollary 1 and 2.

Corollary 1 (Gamma fitted combined signal power): The combined signal power V can be fitted by an equivalent Gamma distributed RV with approximate CDF given by

$$F_V(v) \approx F_{\breve{V}}(v) = \texttt{GamCDF}\left(v, \breve{m}, \breve{\theta}\right), \quad \breve{m} = \left\lfloor \frac{\left(\sum_{i=1}^{2} m_i a_i \theta_i\right)^2}{\sum_{i=1}^{2} m_i \left(a_i \theta_i\right)^2} \right\rfloor, \quad \breve{\theta} = \frac{\sum_{i=1}^{2} m_i a_i \theta_i}{\breve{m}}, \tag{15}$$

where $\breve{m}$ and $\breve{\theta}$ are the fitted shape and scale parameters, and $\lfloor \cdot \rfloor$ rounds down the result.

Proof: This approximation is based on second order moment matching. To be specific, we fit V by $\breve{V}$, which is a Gamma distributed RV with the same first order and second order moments with V. With $\breve{m}$ and $\breve{\theta}$ being the shape and scale parameters of $\breve{V}$, the first and second order moment is $\breve{m}\breve{\theta}$ and $\breve{m}\breve{\theta}^2$, respectively. By fitting the moments with those of V, we have

$$\breve{m}\breve{\theta} = m_1 a_1 \theta_1 + m_2 a_2 \theta_2, \qquad \breve{m}\breve{\theta}^2 = m_1 a_1^2 \theta_1^2 + m_2 a_2^2 \theta_2^2. \tag{16}$$

After some algebraic manipulation, we finally obtain the value of $\breve{m}$ and $\breve{\theta}$, where $\breve{m}$ is rounded down to obtain an integer value. ■

Note that either Lemma 5 or Corollary 1 involves the CDF of Gamma distributed RV, which leads to increased complexity in the analysis on interference. Therefore, we provide another CDF

expression for the combined signal power by approximating the incomplete Gamma function as the weighted sum of exponential functions. The expression is provided in Corollary 2.

Corollary 2 (Alzer's approximate combined signal power): The CDF of the combined signal power V can be approximated as (17) given by

$$F_V(v) \approx 1 - \sum_{n=1}^{\breve{m}} (-1)^{n+1} \binom{\breve{m}}{n} \exp\left(-\frac{n}{\breve{\theta}} (\breve{m}!)^{-\frac{1}{\breve{m}}} v \right). \tag{17}$$

Proof: This corollary follows directly by introducing Alzer's inequality to approximate incomplete Gamma function as the work in [18]. In the approximation, we use the fitted expression in (15) instead of the exact expression in (13). This is because the cumulative terms in (13) are with alternating signs, and Alzer's inequality is invalid under this circumstance. ■

Since the desired signal of V_1, V_2, and V involve Gamma distribution, the Laplace transform (LT) of the interference will be inevitable during the derivation of the outage probability. So we present corresponding results on the LT of interference in next subsection.

C. Laplace Transform of Interference

The interference includes NOMA interference $I_{\mathbf{b}_0}$ from $\mathbf{b}_0$, intra-cluster interference I_{Ψ_0} from Ψ_0, as well as inter-cluster interference I_{Φ_+} from Φ_+. By definition, the LT of I is calculated as $\mathcal{L}_I(s) = \mathbb{E}_I\left[\exp\left(-sI\right)\right]$. The LTs and their high order derivatives are provided in the following Lemma 6, 7, and 8.

Lemma 6 (NOMA interference): The LT of $I_{\mathbf{b}_0}$ denoted by $\mathcal{L}_{I_{\mathbf{b}_0}}(s)$ and its κ-th derivative denoted by $\mathcal{L}^{(\kappa)}_{I_{\mathbf{b}_0}}(s)$ is expressed as (18) and (19), respectively, given by

$$\mathcal{L}_{I_{\mathbf{b}_0}}(s) = \left(1 + \frac{s P_{\mathrm{M}} z_0^{-\alpha_{\mathrm{N}}}}{M m_{\mathrm{N}}} \right)^{-m_{\mathrm{N}}}, \tag{18}$$

$$\mathcal{L}^{(\kappa)}_{I_{\mathbf{b}_0}}(s) = \frac{(m_{\mathrm{N}} + \kappa - 1)!}{(m_{\mathrm{N}} - 1)!} \left(-\frac{P_{\mathrm{M}} z_0^{-\alpha_{\mathrm{N}}}}{M m_{\mathrm{N}}} \right)^{\kappa} \left(1 + \frac{s P_{\mathrm{M}} z_0^{-\alpha_{\mathrm{N}}}}{M m_{\mathrm{N}}} \right)^{-m_{\mathrm{N}} - \kappa}. \tag{19}$$

Proof: The derivation of $\mathcal{L}_{I_{\mathbf{b}_0}}(s)$ is straightforward with $I_{\mathbf{b}_0} = V_1$ being a Gamma distributed RV. Then, by calculating the κ-th derivative, the expression of $\mathcal{L}^{(\kappa)}_{I_{\mathbf{b}_0}}(s)$ can be obtained. ■

Lemma 7 (Intra-cluster interference): Constraining the shortest distance by d_{L} and d_{N} for the interfering LBS and NBS, the LT of the interference from N independent ABSs in I_{Ψ_0} is

calculated as $\mathcal{L}_{I_{\Psi_0}}(s, d_{\mathrm{L}}, d_{\mathrm{N}}, N) = \mathcal{L}^{N}_{I_{\mathbf{d}_{0,n}}}(s, d_{\mathrm{L}}, d_{\mathrm{N}})$, where $\mathcal{L}_{I_{\mathbf{d}_{0,n}}}(s, d_{\mathrm{L}}, d_{\mathrm{N}})$ is the LT of a single interfering ABS in I_{Ψ_0} given by

$$\mathcal{L}_{I_{\mathbf{d}_{0,n}}}(s, d_{\mathrm{L}}, d_{\mathrm{N}}) = \frac{\sum_{\delta\in\{\mathrm{L},\mathrm{N}\}} \int_{d_\delta}^{z_{\mathrm{u}}} f_{Z_{0,n}}(u) p_\delta(u) \left(1 + \frac{sP_{\mathrm{A}}u^{-\alpha_\delta}}{m_\delta}\right)^{-m_\delta} \mathrm{d}u}{\sum_{\nu\in\{\mathrm{L},\mathrm{N}\}} \int_{d_\nu}^{z_{\mathrm{u}}} f_{Z_{0,n}}(u) p_\nu(u) \mathrm{d}u}. \tag{20}$$

The κ-th derivative of $\mathcal{L}_{I_{\Psi_0}}(s, d_{\mathrm{L}}, d_{\mathrm{N}}, N)$ is calculated as

$$\begin{aligned}\mathcal{L}^{(\kappa)}_{I_{\Psi_0}}(s, d_{\mathrm{L}}, d_{\mathrm{N}}, N) = &\sum_{(n_1,\cdots,n_\kappa)\in\mathcal{N}_\kappa(N)} \frac{\kappa!}{\prod_{\tau=1}^{\kappa} n_\tau!} \frac{N!}{(N-K_\kappa)!} \\ &\times \mathcal{L}^{N-K_\kappa}_{I_{\mathbf{d}_{0,n}}}(s, d_{\mathrm{L}}, d_{\mathrm{N}}) \prod_{\tau=1}^{\kappa} \left(\frac{\mathcal{L}^{(\tau)}_{I_{\mathbf{d}_{0,n}}}(s, d_{\mathrm{L}}, d_{\mathrm{N}})}{\tau!}\right)^{n_\tau},\end{aligned} \tag{21}$$

where $\mathcal{N}_\kappa(N)$ is the set of κ-element non-negative integer tuple $(n_1, \cdots, n_\kappa)$ satisfying $\sum_{\tau=1}^{\kappa} \tau \cdot n_\tau = \kappa$ and $K_\kappa = \sum_{\tau=1}^{\kappa} n_\tau \le N$, and the κ-th derivative of $\mathcal{L}_{I_{\mathbf{d}_{0,n}}}(s, d_{\mathrm{L}}, d_{\mathrm{N}})$ is calculated as

$$\begin{aligned}\mathcal{L}^{(\kappa)}_{I_{\mathbf{d}_{0,n}}}(s, d_{\mathrm{L}}, d_{\mathrm{N}}) = &\frac{1}{\sum_{\nu\in\{\mathrm{L},\mathrm{N}\}} \int_{d_\nu}^{z_{\mathrm{u}}} f_{Z_{0,n}}(u) p_\nu(u) \mathrm{d}u} \sum_{\delta\in\{\mathrm{L},\mathrm{N}\}} \int_{d_\delta}^{z_{\mathrm{u}}} f_{Z_{0,n}}(u) p_\delta(u) \\ &\times \frac{(m_\delta+\kappa-1)!}{(m_\delta-1)!} \left(1 + \frac{sP_{\mathrm{A}}u^{-\alpha_\delta}}{m_\delta}\right)^{-m_\delta-\kappa} \left(-\frac{P_{\mathrm{A}}u^{-\alpha_\delta}}{m_\delta}\right)^{\kappa} \mathrm{d}u.\end{aligned} \tag{22}$$

Proof: See Appendix B. ■

Lemma 6 and 7 provide the LT of the interference in the representative cluster. As for inter-cluster interference, it is consisted of the interference from MBSs and ABSs in Φ_+, which is the union of two disjoint sets, i.e., Ω_+ and Ψ_+. Because of the location dependency between the ABSs and their attaching MBS in each cluster, the inter-cluster interference from Ω_+ and Ψ_+ are highly correlated. The results is provided in the following Lemma 8.

Lemma 8 (Inter-cluster interference): The LT of the inter-cluster interference constituted by MBSs and ABSs from Φ_+ can be calculated as

$$\begin{aligned}\mathcal{L}_{I_{\Phi_+}}(s) = \exp\Bigg(-2\pi\lambda_{\mathrm{M}} \int_0^{\infty} \Bigg(1 - \Bigg(1 + \frac{sP_{\mathrm{M}}\left(r^2 + h_{\mathrm{M}}^2\right)^{-\frac{\alpha_{\mathrm{N}}}{2}}}{m_{\mathrm{N}}}\Bigg)^{-m_{\mathrm{N}}} \\ \times \Bigg(\sum_{\delta\in\{\mathrm{L},\mathrm{N}\}} \int_{\tilde{z}}^{z_{\mathrm{u}}} \left(1 + \frac{sP_{\mathrm{A}}z^{-\alpha_\delta}}{m_\delta}\right)^{-m_\delta} p_\delta(z) f_{Z_{i,n}}(z|r) \mathrm{d}z\Bigg)^{N_{\mathrm{s}}}\Bigg) r\mathrm{d}r\Bigg),\end{aligned} \tag{23}$$

where $\tilde{z}=z_{\mathrm{l}}$ for $0<r<r_{\mathrm{s}}$ and $\tilde{z}=z_{\mathrm{m}}$ for $r\geq r_{\mathrm{s}}$. The κ-th derivative of $\mathcal{L}_{I_{\Phi_+}}(s)$ is

$$\begin{aligned}\mathcal{L}^{(\kappa)}_{I_{\Phi_+}}(s)=&\sum_{(n_1,\cdots,n_\kappa)\in\mathcal{N}_\kappa}\frac{\kappa!\mathcal{L}_{I_{\Phi_+}}(s)}{\prod_{\tau=1}^{\kappa}n_\tau!}\prod_{\tau=1}^{\kappa}\left(\sum_{\upsilon=0}^{\tau}\sum_{(k_1,\cdots,k_\upsilon)\in\mathcal{N}_\upsilon(N_{\mathrm{s}})}\frac{2\pi\lambda_{\mathrm{M}}}{\prod_{\eta=1}^{\upsilon}k_\eta!}\frac{N_{\mathrm{s}}!}{(N_{\mathrm{s}}-K_\upsilon)!}\right.\\&\times\int_0^\infty\prod_{\eta=1}^{\upsilon}\left(\sum_{\delta\in\{\mathrm{L},\mathrm{N}\}}\int_{\tilde{z}}^{z_{\mathrm{u}}}\binom{m_\delta+\eta-1}{m_\delta-1}\left(-\frac{P_{\mathrm{A}}z^{-\alpha_\delta}}{m_\delta}\right)^{\eta}\frac{p_\delta(z)f_{Z_{i,n}}(z|r)}{\left(1+\frac{sP_{\mathrm{A}}z^{-\alpha_\delta}}{m_\delta}\right)^{m_\delta+\eta}}\mathrm{d}z\right)^{k_\eta}\\&\times\binom{m_{\mathrm{N}}+\tau-\upsilon-1}{m_{\mathrm{N}}-1}\left(1+\frac{sP_{\mathrm{M}}\left(r^2+h_{\mathrm{M}}^2\right)^{-\frac{\alpha_{\mathrm{N}}}{2}}}{m_{\mathrm{N}}}\right)^{-m_{\mathrm{N}}-\tau+\upsilon}\left(-\frac{P_{\mathrm{M}}\left(r^2+h_{\mathrm{M}}^2\right)^{-\frac{\alpha_{\mathrm{N}}}{2}}}{m_{\mathrm{N}}}\right)^{\tau-\upsilon}\\&\times\left.\left(\sum_{\delta\in\{\mathrm{L},\mathrm{N}\}}\int_{\tilde{z}}^{z_{\mathrm{u}}}\frac{p_\delta(z)f_{Z_{i,n}}(z|r)}{\left(1+\frac{sP_{\mathrm{A}}z^{-\alpha_\delta}}{m_\delta}\right)^{m_\delta}}\mathrm{d}z\right)^{N_{\mathrm{s}}-K_\upsilon}r\mathrm{d}r\right)^{n_\tau},\end{aligned}\tag{24}$$

where $\mathcal{N}_\upsilon(N_{\mathrm{s}})$ and K_υ follow the same meaning as those in Lemma 7.

Proof: See Appendix C. ■

IV. Performance Analysis

With the distance distribution, association probability, LTs and their high order derivative, we are able to study the system performance, i.e., outage probability and ASE, in this section.

A. Outage Probability

We firstly evaluate the outage probability in the following Theorem 1.

Theorem 1 (Outage probability): In the clustered ABS-assisted CoMP network, the outage probability for $\mathbf{u}$ at $(x_0,0,0)$ is expressed as (25) given by

$$\mathcal{O}_{\mathrm{M}}^{y}(x_0)=1-\sum_{n=0}^{m_{\mathrm{N}}-1}\frac{1}{n!}\left(-\xi_{\mathrm{M}}^{y}\right)^n\sum_{(q_1,q_2)\in\mathcal{Q}_2(n)}\binom{n}{q_1,q_2}\mathcal{L}^{(q_1)}_{I_{\Psi_0}}\left(\xi_{\mathrm{M}}^{y},w_{\mathrm{L}},w_{\mathrm{N}},N_{\mathrm{b}}\right)\mathcal{L}^{(q_2)}_{I_{\Phi_+}}\left(\xi_{\mathrm{M}}^{y}\right),\tag{25}$$

if $\mathbf{u}$ is an MUE. In (25), $y\in\{\mathrm{NC},\mathrm{OC}\}$ for NC and OC, $\epsilon=2^{\varsigma}-1$, $N_{\mathrm{NC}}=N_{\mathrm{s}}-1$, $N_{\mathrm{OC}}=N_{\mathrm{s}}$, $\xi_{\mathrm{M}}^{\mathrm{NC}}=\frac{\epsilon}{\theta_1(\beta_{\mathrm{M}}-\mu\beta_{\mathrm{A}}\epsilon)}$, $\xi_{\mathrm{M}}^{\mathrm{OC}}=\frac{2^{2\varsigma}-1}{\theta_1}$, and $\mathcal{Q}_t(n)$ is a set of t-element non-negative integer tuples, i.e., $(q_1,\cdots,q_t)$, satisfying $\sum_{\tau=1}^{t}q_\tau=n$.

If $\mathbf{u}$ is an enhanced AUE either under NC or in the even slots under OC, the outage probability $\mathcal{O}_{\text{EA}}^{\text{NC}}(x_0)$ and $\mathcal{O}_{\text{EA}}^{\text{OC-A}}(x_0)$ can be expressed as (26) given by

$$\mathcal{O}_k^y(x_0) = \int_{z_\text{l}}^{z_\text{u}} \sum_{i=1}^{2} \sum_{j=1}^{m_i} c_{i,j} \left(-a_i\theta_i\right)^j f_{Z_{0,\star}|k}(r) \left(1 - \sum_{n=0}^{j-1} \frac{1}{n!} \left(-\xi_{k,i}^y\right)^n \right.$$
$$\left. \times \sum_{(q_1,q_2)\in\mathcal{Q}_2(n)} \binom{n}{q_1,q_2} \mathcal{L}_{I_{\Psi_0}}^{(q_1)}\left(\xi_{k,i}^y, r_\text{L}, r_\text{N}, N_\text{s}-1\right) \mathcal{L}_{I_{\Phi_+}}^{(q_2)}\left(\xi_{k,i}^y\right) \right) \mathrm{d}r, \tag{26}$$

where $a_1 = \beta_\text{A} - \beta_\text{M}\epsilon$, $a_2 = 1$ for NC, $a_1 = a_2 = 1$ for the even slots under OC, $\xi_{k,i}^y = \frac{\epsilon}{a_i\theta_i}$, $\theta_2 \in \left\{\bar{\theta}_2, \hat{\theta}_2\right\}$ for LUE and NUE, $r_\text{L} = r$, $r_\text{N} = d_{\text{L,N}}(r)$ for LUE, and $r_\text{L} = d_{\text{N,L}}(r)$, $r_\text{N} = r$ for NUE.

If $\mathbf{u}$ is either a regular AUE or an enhanced AUE in the odd slots under OC, the outage probability $\mathcal{O}_{\text{RA}}^{\text{NC}}(x_0)$, $\mathcal{O}_{\text{RA}}^{\text{OC}}(x_0)$, and $\mathcal{O}_{\text{EA}}^{\text{OC-M}}(x_0)$ is expressed as (27) given by

$$\mathcal{O}_k^y(x_0) = 1 - \int_{z_\text{l}}^{z_\text{u}} \sum_{n=0}^{m_k-1} \frac{1}{n!} \left(-\xi_{k,2}^y\right)^n f_{Z_{0,\star}|k}(r) \sum_{(q_1,\cdots,q_3)\in\mathcal{Q}_3(n)} \binom{n}{q_1,\cdots,q_3}$$
$$\times \mathcal{L}_{I_{\mathfrak{b}_0}}^{(q_1)}\left(\xi_{k,2}^y\right) \mathcal{L}_{I_{\Psi_0}}^{(q_2)}\left(\xi_{k,2}^y, r_\text{L}, r_\text{N}, N_\text{s}-1\right) \mathcal{L}_{I_{\Phi_+}}^{(q_3)}\left(\xi_{k,2}^y\right) \mathrm{d}r, \tag{27}$$

where $\xi_{k,2}^y = \frac{\epsilon}{\theta_2}$, $\theta_2 \in \left\{\bar{\theta}_2, \hat{\theta}_2\right\}$ for LUE and NUE, $r_\text{L} = r$, $r_\text{N} = d_{\text{L,N}}(r)$ for LUE, and $r_\text{L} = d_{\text{N,L}}(r)$, $r_\text{N} = r$ for NUE.

Proof: See Appendix D. ■

It can be seen in (25), (26), and (27) that the complexity in calculating the outage probability mainly comes from the partial fraction expansion and the high order derivative of the LT. Therefore, we provide following approximate results for the expression of the outage probability, which are based on Corollary 1 and 2.

Corollary 3 (Gamma fitted outage probability): If $\mathbf{u}$ at $(x_0, 0, 0)$ is an enhanced AUE either under NC or in the even slots under OC, the outage probability $\mathcal{O}_{\text{EA}}^{\text{NC}}(x_0)$ and $\mathcal{O}_{\text{EA}}^{\text{OC-A}}(x_0)$ can be approximated by Gamma fitted expression given by

$$\breve{\mathcal{O}}_k^y(x_0) = 1 - \int_{z_\text{l}}^{z_\text{u}} \sum_{n=0}^{\breve{m}-1} \frac{1}{n!} \left(-\breve{\xi}_k^y\right)^n f_{Z_{0,\star}|k}(r) \sum_{(q_1,q_2)\in\mathcal{Q}_2(n)} \binom{n}{q_1,q_2}$$
$$\times \mathcal{L}_{I_{\Psi_0}}^{(q_1)}\left(\breve{\xi}_k^y, r_\text{L}, r_\text{N}, N_\text{s}-1\right) \mathcal{L}_{I_{\Phi_+}}^{(q_2)}\left(\breve{\xi}_k^y\right) \mathrm{d}r, \tag{28}$$

where $\breve{\xi}_k^y = \frac{\epsilon}{\breve{\theta}}$, $\breve{m} = \left\lfloor \frac{\left(\sum_{i=1}^2 m_i a_i \theta_i\right)^2}{\sum_{i=1}^2 m_i (a_i\theta_i)^2} \right\rfloor$, $\breve{\theta} = \frac{\sum_{i=1}^2 m_i a_i \theta_i}{\breve{m}}$, $a_1 = \beta_\text{A} - \beta_\text{M}\epsilon$, $a_2 = 1$ under NC, $a_1 = a_2 = 1$ for even slots under OC, $\theta_2 \in \left\{\bar{\theta}_2, \hat{\theta}_2\right\}$ for LUE and NUE, $r_\text{L} = r$, $r_\text{N} = d_{\text{L,N}}(r)$ for LUE, and $r_\text{L} = d_{\text{N,L}}(r)$, $r_\text{N} = r$ for NUE.

Corollary 4 (Alzer's approximate outage probability): The outage probability for $\mathbf{u}$ at $(x_0, 0, 0)$ is expressed as (29) given by

$$\tilde{\mathcal{O}}_{\mathrm{M}}^{y}(x_0) = 1 - \sum_{n=1}^{m_{\mathrm{N}}} (-1)^{n+1} \binom{m_{\mathrm{N}}}{n} \mathcal{L}_{I_{\Psi_0}}\left(\tilde{\xi}_{\mathrm{M}}^{y}, w_{\mathrm{L}}, w_{\mathrm{N}}, N_{\mathrm{b}}\right) \mathcal{L}_{I_{\Phi_+}}\left(\tilde{\xi}_{\mathrm{M}}^{y}\right), \tag{29}$$

if $\mathbf{u}$ is an MUE. In (29), $y \in \{\mathrm{NC}, \mathrm{OC}\}$, $N_{\mathrm{NC}} = N_{\mathrm{s}} - 1$, $N_{\mathrm{OC}} = N_{\mathrm{s}}$, $\tilde{\xi}_{\mathrm{M}}^{\mathrm{NC}} = n\left(m_{\mathrm{N}}!\right)^{-\frac{1}{m_{\mathrm{N}}}} \frac{\epsilon}{\theta_1(\beta_{\mathrm{M}} - \mu\beta_{\mathrm{A}}\epsilon)}$, and $\tilde{\xi}_{\mathrm{M}}^{\mathrm{OC}} = n\left(m_{\mathrm{N}}!\right)^{-\frac{1}{m_{\mathrm{N}}}} \frac{2^{2\varsigma}-1}{\theta_1}$.

If $\mathbf{u}$ is an enhanced AUE either under NC or in the even slots under OC, the outage probability $\mathcal{O}_{\mathrm{EA}}^{\mathrm{NC}}(x_0)$ and $\mathcal{O}_{\mathrm{EA}}^{\mathrm{OC\text{-}A}}(x_0)$ can be approximated by Alzer's inequality based expression given by

$$\tilde{\mathcal{O}}_{k}^{y}(x_0) = 1 - \int_{z_{\mathrm{l}}}^{z_{\mathrm{u}}} \sum_{n=1}^{\breve{m}} (-1)^{n+1} \binom{\breve{m}}{n} f_{Z_{0,\star}|k}(r) \mathcal{L}_{I_{\Psi_0}}\left(\tilde{\xi}_{k,n}^{y}, r_{\mathrm{L}}, r_{\mathrm{N}}, N_{\mathrm{s}} - 1\right) \mathcal{L}_{I_{\Phi_+}}\left(\tilde{\xi}_{k,n}^{y}\right) \mathrm{d}r, \tag{30}$$

where $\tilde{\xi}_{k,n}^{y} = n(\breve{m}!)^{-\frac{1}{\breve{m}}} \frac{\epsilon}{\breve{\theta}}$, $\breve{m} = \left\lfloor \frac{\left(\sum_{i=1}^{2} m_i a_i \theta_i\right)^2}{\sum_{i=1}^{2} m_i (a_i \theta_i)^2} \right\rfloor$, $\breve{\theta} = \frac{\sum_{i=1}^{2} m_i a_i \theta_i}{\breve{m}}$, $a_1 = \beta_{\mathrm{A}} - \beta_{\mathrm{M}}\epsilon$, $a_2 = 1$ under NC, $a_1 = a_2 = 1$ for even slots under OC, $\theta_2 \in \left\{\bar{\theta}_2, \hat{\theta}_2\right\}$ for LUE and NUE, $r_{\mathrm{L}} = r$, $r_{\mathrm{N}} = d_{\mathrm{L,N}}(r)$ for LUE, and $r_{\mathrm{L}} = d_{\mathrm{N,L}}(r)$, $r_{\mathrm{N}} = r$ for NUE.

Also by Alzer's inequality, if $\mathbf{u}$ is either a regular AUE or an enhanced AUE in the odd slots under OC, the outage probability $\mathcal{O}_{\mathrm{RA}}^{\mathrm{NC}}(x_0)$, $\mathcal{O}_{\mathrm{RA}}^{\mathrm{OC}}(x_0)$, and $\mathcal{O}_{\mathrm{EA}}^{\mathrm{OC\text{-}M}}(x_0)$ can be approximated as

$$\begin{aligned}\tilde{\mathcal{O}}_{k}^{y}(x_0) = 1 - \int_{z_{\mathrm{l}}}^{z_{\mathrm{u}}} \sum_{n=1}^{m_k} (-1)^{n+1} \binom{m_k}{n} f_{Z_{0,\star}|k}(r) \\ \times \mathcal{L}_{I_{\mathrm{b}_0}}\left(\tilde{\xi}_{k,2}^{y}\right) \mathcal{L}_{I_{\Psi_0}}\left(\tilde{\xi}_{k,2}^{y}, r_{\mathrm{L}}, r_{\mathrm{N}}, N_{\mathrm{s}} - 1\right) \mathcal{L}_{I_{\Phi_+}}\left(\tilde{\xi}_{k,2}^{y}\right) \mathrm{d}r,\end{aligned} \tag{31}$$

where $\tilde{\xi}_{k,2}^{y} = n(m_k!)^{-\frac{1}{m_k}} \frac{\epsilon}{\theta_2}$, $\theta_2 \in \left\{\bar{\theta}_2, \hat{\theta}_2\right\}$ for LUE and NUE, $r_{\mathrm{L}} = r$, $r_{\mathrm{N}} = d_{\mathrm{L,N}}(r)$ for LUE, and $r_{\mathrm{L}} = d_{\mathrm{N,L}}(r)$, $r_{\mathrm{N}} = r$ for NUE.

The proof for Corollary 1 and 2 follows by straightly plugging the Gamma fitted CDF expression for the enhanced signal power into the derivation in Theorem 1, and introducing Alzer's inequality to deal with the incomplete Gamma function, respectively. Besides, under OC, the outage probability of enhanced AUE can be obtained by averaging the outage probabilities in the odd and even slots as $\mathcal{O}_{\mathrm{EA}}^{\mathrm{OC}} = \frac{1}{2}\left(\mathcal{O}_{\mathrm{EA}}^{\mathrm{OC\text{-}M}} + \mathcal{O}_{\mathrm{EA}}^{\mathrm{OC\text{-}A}}\right)$.

B. Average Area Outage Spectral Efficiency

As for the ASE, recall that it evaluates the performance from the perspective of system, which is defined as the achievable SE of a unit area given target user SE threshold. We consider dense networking with a large number of UE distributed. Hence, it makes sense to assume that all

MBSs and ABSs are associated with UEs. As a result, the ASE of each cluster includes two components, one from the MBS and the other from the ABSs attached to the MBS. Denoting by $\mathcal{U}^y$ ($y \in \{\text{NC}, \text{OC}\}$) the ASE of the system, it is formally calculated as

$$\mathcal{U}^y = (M + N_\text{s})\,\lambda_\text{M}\varsigma \int_0^{r_\text{s}} \left(1 - \mathcal{O}^y(x_0)\right) f_{D_{i,n}}(x_0)\mathrm{d}x_0, \tag{32}$$

where $\mathcal{O}^y(x_0)$ is the overall outage probability with respect to a typical UE located at $(x_0, 0, 0)$, which takes all association categories into consideration that

$$\mathcal{O}^y(x_0) = \mathcal{A}_\text{M}(x_0)\mathcal{O}^y_\text{M}(x_0) + \sum_{k\in\{\text{L},\text{N}\}} \mathcal{A}_k(x_0)\left(\frac{M}{N_\text{s}}\mathcal{O}^y_{\text{E}k}(x_0) + \frac{N_\text{s} - M}{N_\text{s}}\mathcal{O}^y_{\text{R}k}(x_0)\right). \tag{33}$$

In (33), E$k \in \{\text{EL}, \text{EN}\}$ for enhanced LUE and NUE, and R$k \in \{\text{RL}, \text{RN}\}$ for regular LUE and NUE. Also note that the integral in (32) averages over all possible locations of the typical UE. Finally, by plugging (25), (26), and (27) into (33) and then (32), we can evaluate the ASE of the system. Likewise, by averaging $\mathcal{O}^y(x_0)$ over x_0, we can also calculate the area outage probability of the system denoted by $\mathcal{O}^y$ ($y \in \{\text{NC}, \text{OC}\}$).

C. Comparison with the OMA based CoMP

Intuitively, splitting transmit power to support CoMP transmission for AUE will lead to quality degradation in the received signal of MUE. However, this recognition can be misleading, because NOMA can overtake OMA from the perspective of outage probability for MUE under certain condition. Such condition is presented in the following Corollary 5.

Corollary 5 (NOMA superiority over OMA for MUE): The outage probability for MUE under NC is lower than that under OC if the NOMA power allocation coefficient β_A, the target SE ς, and the SIC residual interference ratio μ satisfy the condition that

$$\max\left(\frac{2^\varsigma - 1}{2^\varsigma}, 0.5\right) < \beta_\text{A} < \frac{2^\varsigma}{2^\varsigma + 1 + \mu\left(2^{2\varsigma} - 1\right)}. \tag{34}$$

Proof: As revealed in Theorem 1, $\beta_\text{A} > \beta_\text{M}\left(2^\varsigma - 1\right)$ should be satisfied to realize effective joint transmission, which yields the condition that $\beta_\text{A} > \frac{2^\varsigma - 1}{2^\varsigma}$. Then, with the SIR for MUE under NC in (3), we have

$$\mathcal{O}^\text{NC}_\text{M} < \mathbb{P}\left(V_1 < \frac{\left(2^\varsigma - 1\right) I}{\beta_\text{M} - \mu\beta_\text{A}\left(2^\varsigma - 1\right)}\right), \tag{35}$$

where $I = I_{\Psi_0} + I_{\Omega_+} + I_{\Psi_+}$ and $I_{\Psi_0} = \sum_{\mathbf{d}_{0,n}\in\Psi_0} \frac{P_\text{A} h^2_{0,n}}{Z^\alpha_{0,n}} > \sum_{n=1}^{N_\text{s}-1} \frac{P_\text{A} h^2_{0,n}}{Z^\alpha_{0,n}}$. As for the case under OC, we have $\mathcal{O}^\text{OC}_\text{M} = \mathbb{P}\left(V_1 < \left(2^{2\varsigma} - 1\right) I\right)$. Evidently, if $\left(2^{2\varsigma} - 1\right) > \frac{\left(2^\varsigma - 1\right)}{\beta_\text{M} - \mu\beta_\text{A}\left(2^\varsigma - 1\right)}$, then $\mathcal{O}^\text{NC}_\text{M} < \mathcal{O}^\text{OC}_\text{M}$ will be guaranteed. After some algebraic manipulation, the condition in (34) can be reached. ■

V. Numerical Results and Discussions

In this section, we firstly validate our theoretical outage probability expressions under different propagation environments. Then, we study the impacts of main system parameters including the ABS height and ABS number. Finally, we also compare the outage probability and ASE under NC with those under OC to investigate the superiority of NOMA over OMA in realizing cross-tier CoMP transmission.

Both theoretical and Monte Carlo simulation based results are obtained through Matlab. Assuming dense urban environment, we set $b = 0.114$ and $c = 12.08$ as in [30] to determine LoS and NLoS propagation for air-to-ground links. The density and height of MBSs is $\lambda_{\mathrm{M}} = 1$ BSs per square km and $h_{\mathrm{M}} = 10$ m, and the traffic offloading bias is fixed as $B = 0.3$. The transmit power is 43 dBm for MBSs and 37 dBm for ABSs. The ABS cluster size and SIC residual interference ratio is $r_{\mathrm{s}} = 400$ m and $\mu = 0.01$, respectively. These parameter settings are slight modifications of those appeared in [24], [33], and [34]. Unless otherwise stated, please find the detailed parameters in the caption of the figure.

A. Accuracy Validation

In Fig. 2a and Fig. 2b, we firstly validate our exact theoretical outage probability expressions provided in Theorem 1, as well as the approximated expressions provided in Corollary 3 and 4. The theoretical results are compared with those obtained through Monte Carlo simulation, which are averaged over 100000 independent runs in a circular area with a radius of 50 km.

Fig. 2a plots the outage probabilities $\mathcal{O}_{\mathrm{M}}^{\mathrm{NC}}(x_0)$, $\mathcal{O}_{\mathrm{L}}^{\mathrm{NC}}(x_0)$, $\mathcal{O}_{\mathrm{N}}^{\mathrm{NC}}(x_0)$, and $\mathcal{O}^{\mathrm{NC}}(x_0)$ for NC with the target SE ς given $\alpha_{\mathrm{L}} = 2.8$, $\alpha_{\mathrm{N}} = 3.2$, and $x_0 = 70$ m. The figure shows that our exact theoretical results perfectly match the Monte Carlo simulation based results for all association cases under $\{m_{\mathrm{L}}, m_{\mathrm{N}}\} = \{4, 2\}$. It also demonstrates that the Gamma fitted expressions are highly reliable with negligible mismatch. Fig. 2b plots the outage probabilities $\mathcal{O}^{\mathrm{NC}}(x_0)$ for NC with the distance x_0 given target SE $\varsigma = 0.5$ bps/Hz. This figure also validates our exact expressions and shows that the accuracy of the Gamma fitted expressions is insensitive to varying path-loss exponents, i.e., $\{\alpha_{\mathrm{L}}, \alpha_{\mathrm{N}}\} = \{2.8, 3.2\} \rightarrow \{2.2, 2.6\}$.

Both Fig. 2a and 2b present observable gaps between the Alzer's approximate results and the exact results, especially for the LUEs. This indicates that the theoretical analysis will be less accurate for a wide range of distance x_0 if low complexity is maintained through Alzer's inequality. On the other hand, it turns out that increased m_{L}, i.e., $m_{\mathrm{L}} = 4 \rightarrow 6$, has minor

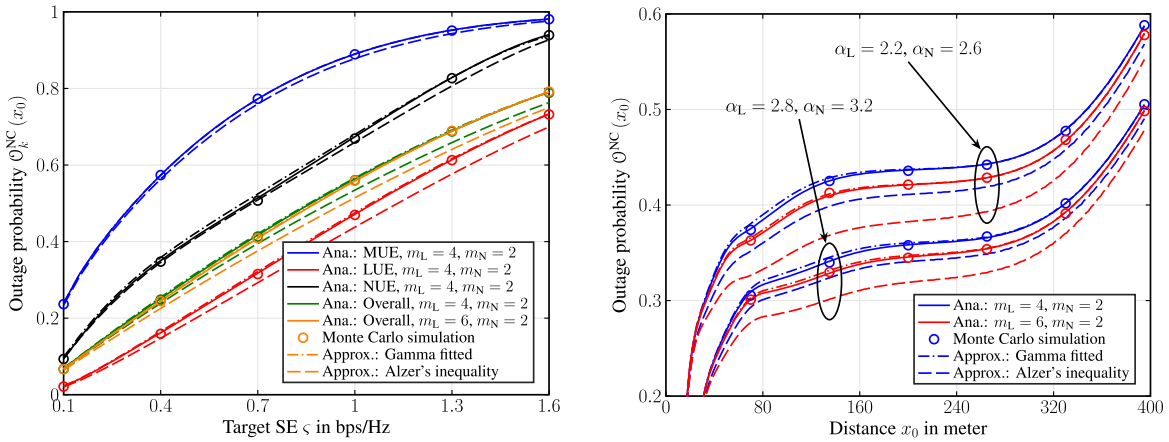

(a) Accuracy validation against varying target SE ς with $\alpha_{\mathrm{L}}=2.8$, $\alpha_{\mathrm{N}}=3.2$, and $x_0=70$ m.

(b) Accuracy validation against varying distance x_0 with target SE $\varsigma=0.5$ bps/Hz.

Fig. 2. Outage probabilities $\mathcal{O}_k^{\mathrm{NC}}(x_0)$ and $\mathcal{O}^{\mathrm{NC}}(x_0)$ vs. target SE ς and distance x_0 under various propagation environment with $\beta_{\mathrm{A}}=0.7$, $h_{\mathrm{A}}=80$ m, $M=8$, and $N_{\mathrm{s}}=10$.

influence over the outage performance, but the accuracy will be further reduced for the Alzer's approximate expressions. Upon above discussion, we will mainly resort to the Gamma fitted expressions in the following Subsection V-B and V-C and focus on propagation parameter setting $\{\alpha_{\mathrm{L}},\alpha_{\mathrm{N}}\}=\{2.8,3.2\}$ and $\{m_{\mathrm{L}},m_{\mathrm{N}}\}=\{4,2\}$[6].

B. Impacts of System Parameters

Based on the derived analytical expressions, we will now study the impacts of various parameters including the ABS height, ABS number, and antenna number. The investigation in this subsection is performed under fixed NOMA power allocation coefficient $\beta_{\mathrm{A}}=0.7$.

Fig. 3a plots the outage probability $\mathcal{O}^{\mathrm{NC}}(x_0)$ with the ABS height h_{A} for UEs located at different locations given $\varsigma=0.5$ bps/Hz. The figure shows that deploying more ABSs will cause degradation in outage probability for cell-center UEs, i.e., $x_0=50$ m. This indicates that, the increase in desired signal power from the ABS due to shortened link distance and higher LoS probability is insignificant and cannot overtake the deteriorated aggregate interference from other ABSs. But for cell-edge UEs, i.e., $x_0=350$ m, when the ABSs are deployed at lower altitude, adding more ABSs can be beneficial because the desired signal power will rapidly increase for

[6]Another reason for limiting $m\leq 4$ originates from the work in [35], which provides relative results through field test in suburban and near-urban environments.

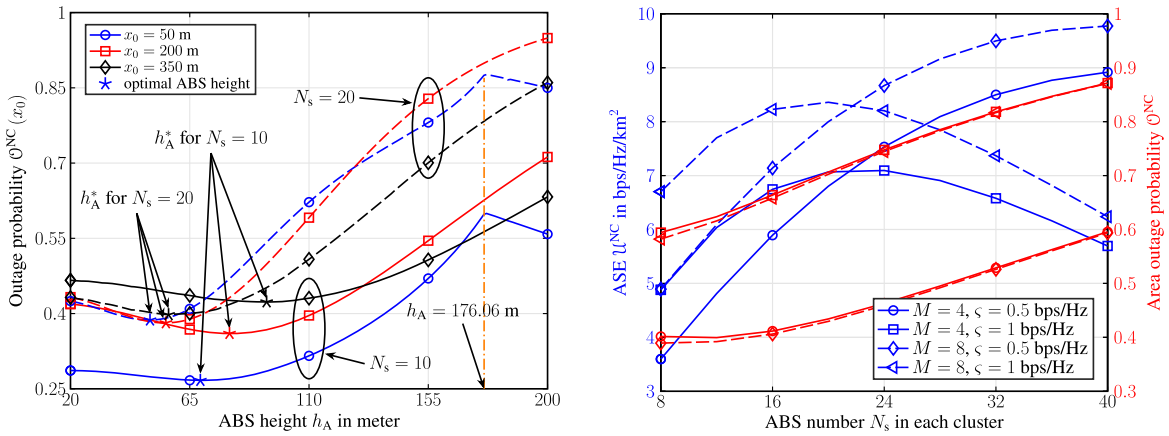

(a) Impacts of ABS height h_A with target SE $\varsigma = 0.5$ bps/Hz.

(b) Impacts of ABS number N_s in each cluster and antenna number M with ABS height $h_A = 80$ m.

Fig. 3. Outage probability $\mathcal{O}^{NC}(x_0)$ and $\mathcal{O}^{NC}$, and ASE $\mathcal{U}^{NC}$ vs. ABS height h_A and ABS number N_s with $\beta_A = 0.7$.

these UEs. The figure also presents an optimal ABS height h_A^* for each curve, respectively, which leads to the lowest outage probability. The cell-center UE and cell-edge UE share different h_A^*, though the difference becomes less distinguishable when more ABSs are introduced in each cluster. In addition, an inflection point at $h_A \approx 176$ m can be observed for the UE at $x_0 = 50$ m. This is due to the change in SIR structure, because beyond this height these UEs will certainly be associated with the MBS according to the association policy.

Fig. 3b plots the ASE $\mathcal{U}^{NC}$ and area outage probability $\mathcal{O}^{NC}$ with the ABS number N_s. It can be observed that when fewer ABSs are deployed in each cluster, e.g., $N_s = 16$, targeting higher SE in each communication link brings in better ASE performance for the system. But in dense ABS deployment scenario, e.g., $N_s = 30$, high target SE leads to dramatical ASE decrease with the growth of ABS number. This is because the area outage probability under high target SE has reached an outrageous level, e.g., $\mathcal{O}^{NC} > 0.7$, with ABS densely deployed, sparing no room for any improvement in the ASE. Fig. 3b also shows the benefit of equipping the MBSs with more transmit antennas from the aspect of ASE. This is due to the linear increase in the number of data streams while maintaining a similar area outage probability.

C. Superiority of NOMA Enabled CoMP

In this subsection, we firstly compare the outage probability of NC for different type of UE with that of OC in Fig. 4.

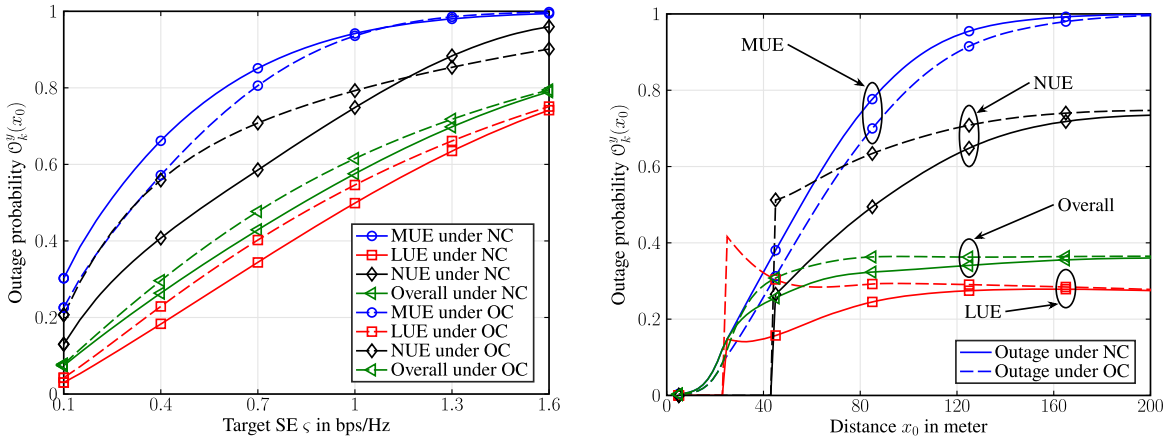

(a) Outage probability vs target SE ς with $x_0 = 80$ m.

(b) Outage probability vs x_0 with $\varsigma = 0.5$ bps/Hz.

Fig. 4. Outage probability comparison between NC and OC with $\beta_{\mathrm{A}} = 0.7$, $M = 8$, $h_{\mathrm{A}} = 80$ m, and $N_{\mathrm{s}} = 10$.

Fig. 4a plots the outage probability $\mathcal{O}_k^y(x_0)$ of the MUE, LUE, and NUE under NC and OC with the target SE ς given $x_0 = 80$ m. The results present improved outage performance for the LUE and NUE under NC within a wide range of target SE, e.g., $\varsigma < 1.1$ bps/Hz. In low target SE regime, the benefit of NC is more obvious for the NUE. This is because the received signal power at the NUE is also enhanced in odd slots under NC, which greatly increases the chance of successful transmission on average. But for the LUE, the improvement is less obvious. This is due to the fact that the LUE can receive strong LoS signal from its associated LBS, which puts less emphasis on the benefit of joint transmission. It also shows that, in high target SE regime, OC takes advantage over NC for the NUE, because the assisting MBS jointly transmits with full power in the even slots under OC to meet with the rigorous target SE. At last, a better overall outage performance is still expectable under NC, though splitting transmit power brings in negative impact for the MUE.

Fig. 4b verifies the advantage of NC over OC in outage probability with varying distance x_0 given $\varsigma = 0.5$ bps/Hz. We focus on $0 < x_0 < 200$, though the cluster size is set as $r_{\mathrm{s}} = 400$ m, since the fluctuation in outage probability is not obvious when $x_0 > 200$. Likewise, the results show that NC brings in significant decrease in outage probability for the LUE and NUE. This improvement surpasses the outage performance degradation in the MUE, as the overall outage probability is lower under NC than OC. It can also be observed that the outage probability is zero either for the LUE with $x_0 < 25$ m or for the NUE with $x_0 < 44$ m. This is because within such range of x_0, UEs will certainly be associated with the MBS, since the ABS height

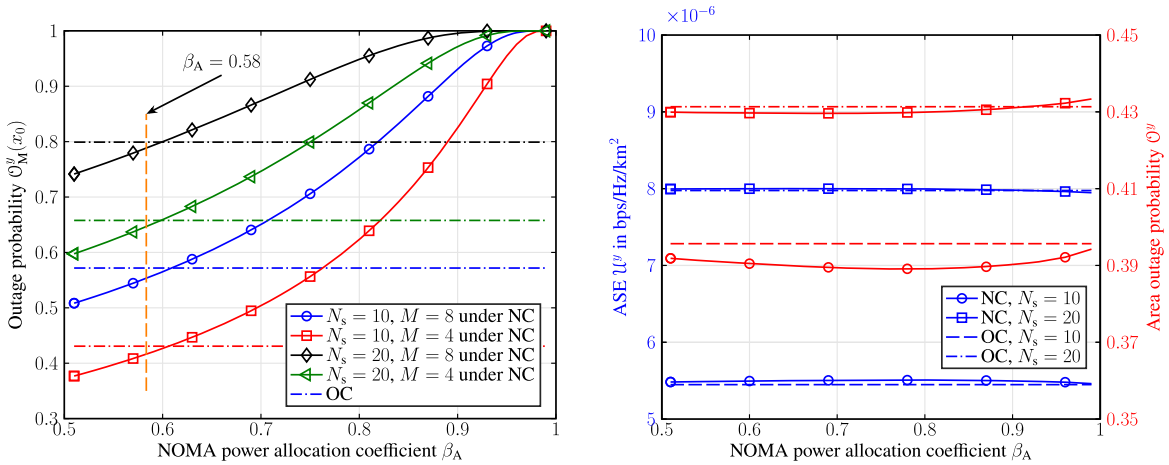

(a) Outage probability of MUE vs NOMA power allocation coefficient β_A with $\varsigma = 0.5$ bps/Hz and $x_0 = 80$ m.

(b) ASE and area outage probability vs NOMA power allocation coefficient β_A with $\varsigma = 0.5$ bps/Hz and $M = 8$.

Fig. 5. Impact of NOMA power allocation coefficient on the superiority of NC with $h_A = 80$ m.

$h_A = 80$ m limits the maximal average received signal power from the ABSs. It should also be noted that when $x_0 < 50$ m, the outage probability of the LUE will decrease with x_0, which is different from the trend for that of the NUE and the MUE. This is the result of traffic offloading, which prohibits the LUEs from being associated with the BS providing the strongest received signal power in small x_0 region. In consequence, moving away from the MBS results in lower interference level for the regular LUE in this region, and thus improves the reliability of the link.

Finally, we investigate the impact of NOMA power allocation coefficient on the superiority of NC in Fig. 5.

In Fig. 5a, the outage probability $\mathcal{O}_M^y(x_0)$ of the MUE with NOMA power allocation coefficient β_A is illustrated for NC and OC. The results show that with the increase of β_A, more power is allocated to assist the joint transmission for LUEs, thus leading to deteriorated outage performance for the MUE. However, if β_A is carefully selected, NC can still guarantee a lower outage probability for the MUE than OC. Under $\mu = 0.01$ and $\varsigma = 0.5$ bps/Hz, the sufficient condition $\beta_A \leq 0.58$ calculated according to Corollary 5 is also plotted in Fig. 5a. It should be noted that $\beta_A \leq 0.58$ is sufficient but not necessary, thus illustrating a small gap in the figure. The advantage of NC for the MUE originates from the fact that the MUE has twice the time resource in NC compared with OC, which neutralizes the negative impact of splitting transmit

power. The results also exhibit higher outage probability for the MUE with more ABSs and more parallel data streams.

Fig. 5b investigates the overall system performance, i.e., the ASE $\mathcal{U}^y$ and area outage probability $\mathcal{O}^y$, for NC and OC under different ABS number $N_{\rm s}$ for each cluster with varying NOMA power allocation coefficient $\beta_{\rm A}$. The results show that, NC brings in better ASE and area outage probability performance for a wide range of $\beta_{\rm A}$. The performance gains in both metrics are not obvious, which is because the cluster size is fixed as $r_{\rm s} = 400$ m and the benefit of cross-tier joint transmission is insignificant in large x_0 regime.

VI. Conclusion

This paper considers a non-orthogonal cross-tier joint transmission framework for clustered ABS-assisted networks. In such system, each MBS applies ZF-BF to provide multiple parallel data streams and utilizes NOMA to multiplex the signals for a scheduling MUE and an active AUE in each stream, while each ABS solely transmits signal to its scheduling AUE. Consequently, CoMP is implemented without violating the original purpose of network densification. Under a MCP based random network topology, we theoretically investigate the outage probability and area outage spectral efficiency of the focused non-orthogonal cross-tier joint transmission framework. Numerical results reveal that, NOMA enabled CoMP framework exploits subchannel resources in a more efficient way, compared with its OMA based counterpart, and thus brings in improved outage and spectral efficiency performance.

The work in this paper also allows several extensions in the future. The first is applying other advanced physical transmission techniques, e.g., rate splitting multiple access, to realize a more flexible combination of ZF-BF and NC-JT. Secondly, the performance evaluation can also be extended to investigate the influence of direction misalignment between the pairing UEs. Another promising extension lies in designing efficient coordinating BS selection strategy considering that the benefit of joint transmission naturally diminishes for the UEs served by the cluster-edge ABSs.

Appendix A
Proof of Lemma 5

Recall that $\mathbf{w}_m$ is the ZF-BF vector and $P_{\rm M}$ is equally divided between M streams. Thus, we can reach that $V_i \overset{\rm d}{\sim} \mathrm{Gamma}\left(m_i, \theta_i\right)$ under Nakagami-m fading assumption.

Then, we deal with the CDF of V, which turns out to be the weighted sum of two independent Gamma distributed RVs with non-identical scale parameters. To this end, we resort to the moment generating function (MGF) of V, which is calculated as

$$\mathcal{M}_V(s) = \mathbb{E}_{V_1,V_2}\left[\exp\left(s\left(a_1V_1 + a_2V_2\right)\right)\right] = \left(1 - a_1\theta_1 s\right)^{-m_1}\left(1 - a_2\theta_2 s\right)^{-m_2}. \tag{36}$$

By partial fraction expansion, $\mathcal{M}_V(s)$ can be rewritten as

$$\mathcal{M}_V(s) = \sum_{i=1}^{2}\sum_{j=1}^{m_i} c_{i,j}\left(s - \frac{1}{a_i\theta_i}\right)^{-j}, \tag{37}$$

where $c_{i,j}$ is calculated as

$$c_{i,j} = \frac{1}{(m_i - j)!}\left(-\frac{1}{a_i\theta_i}\right)^{m_i}\left[\frac{\mathrm{d}^{m_i-j}}{\mathrm{d}s^{m_i-j}}\mathcal{M}_V(s)\cdot\left(1 - a_i\theta_i s\right)^{m_i}\right]\Bigg|_{s\to\frac{1}{a_i\theta_i}}. \tag{38}$$

It should be noted that calculating $c_{i,j}$ involves the high order derivative of $\mathcal{M}_V(s)$. After some algebraic manipulation, we obtain the expression of $c_{i,j}$ in (14). Obviously, $\mathcal{M}_V(s)$ in (37) is the linear combination of multiple MGFs of Gamma distributed RVs. Thus, we can reach the expression of the CDF of V in (13) according to the linear transform relationship between the MGF and CDF of Gamma distributed RVs.

APPENDIX B
PROOF OF LEMMA 7

By definition, $\mathcal{L}_{I_{\mathbf{d}_{0,n}}}(s, d_{\mathrm{L}}, d_{\mathrm{N}})$ is calculated as

$$\begin{aligned}\mathcal{L}_{I_{\mathbf{d}_{0,n}}}(s, d_{\mathrm{L}}, d_{\mathrm{N}}) &= \mathbb{E}\left[\exp\left(-sP_{\mathrm{A}}Z_{0,n}^{-\alpha}h_{0,n}^2\right)\right]\\ &= \frac{\mathbb{P}\left(\mathbf{d}_{0,n} = \bar{\mathbf{d}}_{0,n}, \bar{Z}_{0,n} > d_{\mathrm{L}}\right)\cdot\mathbb{E}\left[\exp\left(-sP_{\mathrm{A}}\bar{Z}_{0,n}^{-\alpha_{\mathrm{L}}}\bar{h}_{0,n}^2\right)\right]}{\mathbb{P}\left(\mathbf{d}_{0,n} = \bar{\mathbf{d}}_{0,n}, \bar{Z}_{0,n} > d_{\mathrm{L}}\right) + \mathbb{P}\left(\mathbf{d}_{0,n} = \hat{\mathbf{d}}_{0,n}, \hat{Z}_{0,n} > d_{\mathrm{N}}\right)}\\ &\quad + \frac{\mathbb{P}\left(\mathbf{d}_{0,n} = \hat{\mathbf{d}}_{0,n}, \hat{Z}_{0,n} > d_{\mathrm{N}}\right)\cdot\mathbb{E}\left[\exp\left(-sP_{\mathrm{A}}\hat{Z}_{0,n}^{-\alpha_{\mathrm{N}}}\hat{h}_{0,n}^2\right)\right]}{\mathbb{P}\left(\mathbf{d}_{0,n} = \bar{\mathbf{d}}_{0,n}, \bar{Z}_{0,n} > d_{\mathrm{L}}\right) + \mathbb{P}\left(\mathbf{d}_{0,n} = \hat{\mathbf{d}}_{0,n}, \hat{Z}_{0,n} > d_{\mathrm{N}}\right)},\end{aligned} \tag{39}$$

where in (39) we have

$$\begin{aligned}\mathbb{P}\left(\mathbf{d}_{0,n} = \bar{\mathbf{d}}_{0,n}, \bar{Z}_{0,n} > d_{\mathrm{L}}\right) &= \int_{d_{\mathrm{L}}}^{z_{\mathrm{u}}} f_{Z_{0,n}}(u)p_{\mathrm{L}}(u)\mathrm{d}u,\\ \mathbb{P}\left(\mathbf{d}_{0,n} = \hat{\mathbf{d}}_{0,n}, \hat{Z}_{0,n} > d_{\mathrm{N}}\right) &= \int_{d_{\mathrm{N}}}^{z_{\mathrm{u}}} f_{Z_{0,n}}(u)p_{\mathrm{N}}(u)\mathrm{d}u.\end{aligned} \tag{40}$$

By plugging above two equations and the MGF of Gamma distributed RV into (39), we can reach the expression of $\mathcal{L}_{I_{\mathbf{d}_{0,n}}}(s, d_{\mathrm{L}}, d_{\mathrm{N}})$ in (20). The expression of $\mathcal{L}^{(\kappa)}_{I_{\mathbf{d}_{0,n}}}(s, d_{\mathrm{L}}, d_{\mathrm{N}})$ in (22) can be directly obtained by calculating the κ-th derivative of (20).

Given that $\mathcal{L}_{I_{\Psi_0}}(s, d_{\mathrm{L}}, d_{\mathrm{N}}, N)$ is the LT of the aggregate interference from N independent $\mathbf{d}_{0,n}$, its expression can be obtained by calculating the N-power of $\mathcal{L}_{I_{\mathbf{d}_{0,n}}}(s, d_{\mathrm{L}}, d_{\mathrm{N}})$.

Finally, it is shown that $\mathcal{L}_{I_{\Psi_0}}(s, d_{\mathrm{L}}, d_{\mathrm{N}}, N)$ holds the form of composite function $f(g(x))$, where $f(x) = x^N$ and $g(x) = \mathcal{L}_{I_{\mathbf{d}_{0,n}}}(x, d_{\mathrm{L}}, d_{\mathrm{N}})$. So with Faà di Bruno's formula that

$$\frac{\mathrm{d}^\kappa}{\mathrm{d}s^\kappa} f(g(x)) = \sum_{(n_1,\cdots,n_\kappa)\in\mathcal{N}_\kappa} \frac{\kappa!}{\prod_{\tau=1}^{\kappa} n_\tau!} f^{(n_1+\cdots+n_\kappa)}(g(x)) \prod_{\tau=1}^{\kappa} \left(\frac{g^{(\tau)}(x)}{\tau!}\right)^{n_\tau}, \tag{41}$$

and

$$\frac{\mathrm{d}^\kappa}{\mathrm{d}x^\kappa} f(x) = \begin{cases} \dfrac{N!}{(N-\kappa)!} x^{N-\kappa}, & \kappa \le N, \\ 0, & \kappa > N, \end{cases} \tag{42}$$

we can reach the expression of $\mathcal{L}^{(\kappa)}_{I_{\Psi_0}}(s, d_{\mathrm{L}}, d_{\mathrm{N}}, N)$ in (21).

APPENDIX C
PROOF OF LEMMA 8

By definition, $\mathcal{L}_{I_{\Phi_+}}(s)$ is calculated as

$$\begin{aligned}
\mathcal{L}_{I_{\Phi_+}}(s) &= \mathbb{E}\left[\exp\left(-s\sum_{\mathbf{b}_i\in\Omega_+}\left(P_{\mathrm{M}} Z_i^{-\alpha_{\mathrm{N}}} \left|\mathbf{h}_i \mathbf{w}_{i,m}\right|^2 + \sum_{\mathbf{d}_{i,n}\in\Psi_i} P_{\mathrm{A}} Z_{i,n}^{-\alpha} h_{i,n}^2\right)\right)\right] \\
&= \mathbb{E}\left[\prod_{\mathbf{b}_i\in\Omega_+}\left(\exp\left(-sP_{\mathrm{M}} Z_i^{-\alpha_{\mathrm{N}}} \left|\mathbf{h}_i \mathbf{w}_{i,m}\right|^2\right) \prod_{\mathbf{d}_{i,n}\in\Psi_i} \exp\left(-sP_{\mathrm{A}} Z_{i,n}^{-\alpha} h_{i,n}^2\right)\right)\right] \\
&\overset{(a)}{=} \mathbb{E}\left[\prod_{\mathbf{b}_i\in\Omega_+}\left(\left(1+\frac{sP_{\mathrm{M}}\left(R_i^2+h_{\mathrm{M}}^2\right)^{-\frac{\alpha_{\mathrm{N}}}{2}}}{m_{\mathrm{N}}}\right)^{-m_{\mathrm{N}}} \left(\sum_{\delta\in\{\mathrm{L},\mathrm{N}\}} \int_{\tilde{z}}^{z_{\mathrm{u}}} \frac{p_\delta(z) f_{Z_{i,n}}(z|R_i)}{\left(1+\frac{sP_{\mathrm{A}} z^{-\alpha_\delta}}{m_\delta}\right)^{m_\delta}} \mathrm{d}z\right)^{N_{\mathrm{s}}}\right)\right],
\end{aligned} \tag{43}$$

where (a) is due to the MGF of Gamma distributed RV. Following from the probability generating functional of PPP [29], we can reach the expression of $\mathcal{L}_{I_{\Phi_+}}(s)$ in (23).

Evidently, $\mathcal{L}_{I_{\Phi_+}}(s)$ is also in the form of composite function $f(g(x))$ with $f(x)=\exp(x)$ and

$$g(x)=-2\pi\lambda_{\mathrm{M}}\int_0^{\infty}\left(1-\left(1+\frac{xP_{\mathrm{M}}\left(r^2+h_{\mathrm{M}}^2\right)^{-\frac{\alpha_{\mathrm{N}}}{2}}}{m_{\mathrm{N}}}\right)^{-m_{\mathrm{N}}}\times\left(\sum_{\delta\in\{\mathrm{L},\mathrm{N}\}}\int_{\tilde{z}}^{z_{\mathrm{u}}}\frac{p_\delta(z)f_{Z_{i,n}}(z|r)}{\left(1+\frac{xP_{\mathrm{A}}z^{-\alpha_\delta}}{m_\delta}\right)^{m_\delta}}\mathrm{d}z\right)^{N_{\mathrm{s}}}\right)r\mathrm{d}r. \tag{44}$$

So by utilizing Faà di Bruno's formula in (41), we have

$$\begin{aligned}\mathcal{L}_{I_{\Phi_+}}^{(\kappa)}(s)&=\sum_{(n_1,\cdots,n_\kappa)\in\mathcal{N}_\kappa}\frac{\kappa!f^{(n_1+\cdots+n_\kappa)}(g(s))}{\prod_{\tau=1}^{\kappa}n_\tau!}\prod_{\tau=1}^{\kappa}\left(\frac{g^{(\tau)}(s)}{\tau!}\right)^{n_\tau}\\&=\sum_{(n_1,\cdots,n_\kappa)\in\mathcal{N}_\kappa}\frac{\kappa!\mathcal{L}_{I_{\Phi_+}}(s)}{\prod_{\tau=1}^{\kappa}n_\tau!}\prod_{\tau=1}^{\kappa}\left(\frac{g^{(\tau)}(s)}{\tau!}\right)^{n_\tau}.\end{aligned} \tag{45}$$

It should be noted that (45) involves the τ-th derivative of $g(s)$, which is calculated as

$$\begin{aligned}g^{(\tau)}(s)&=2\pi\lambda_{\mathrm{M}}\int_0^{\infty}\left[\frac{\mathrm{d}^\tau}{\mathrm{d}s^\tau}\left(1+\frac{sP_{\mathrm{M}}\left(r^2+h_{\mathrm{M}}^2\right)^{-\frac{\alpha_{\mathrm{N}}}{2}}}{m_{\mathrm{N}}}\right)^{-m_{\mathrm{N}}}\right.\\&\quad\left.\times\left(\sum_{\delta\in\{\mathrm{L},\mathrm{N}\}}\int_{\tilde{z}}^{z_{\mathrm{u}}}\frac{p_\delta(z)f_{Z_{i,n}}(z|r)}{\left(1+\frac{sP_{\mathrm{A}}z^{-\alpha_\delta}}{m_\delta}\right)^{m_\delta}}\mathrm{d}z\right)^{N_{\mathrm{s}}}\right]r\mathrm{d}r\\&=2\pi\lambda_{\mathrm{M}}\int_0^{\infty}\left[\frac{\mathrm{d}^\tau}{\mathrm{d}s^\tau}b(s)h(e(s))\right]r\mathrm{d}r=2\pi\lambda_{\mathrm{M}}\sum_{\upsilon=0}^{\tau}\binom{\tau}{\upsilon}\int_0^{\infty}b^{(\tau-\upsilon)}(s)\left[\frac{\mathrm{d}^\upsilon}{\mathrm{d}s^\upsilon}h(e(s))\right]r\mathrm{d}r,\end{aligned} \tag{46}$$

where $h(x)=x^{N_{\mathrm{s}}}$ and

$$b(x)=\left(1+\frac{xP_{\mathrm{M}}\left(r^2+h_{\mathrm{M}}^2\right)^{-\frac{\alpha_{\mathrm{N}}}{2}}}{m_{\mathrm{N}}}\right)^{-m_{\mathrm{N}}}, \tag{47}$$

$$e(x)=\sum_{\delta\in\{\mathrm{L},\mathrm{N}\}}\int_{\tilde{z}}^{z_{\mathrm{u}}}p_\delta(z)f_{Z_{i,n}}(z|r)\left(1+\frac{xP_{\mathrm{A}}z^{-\alpha_\delta}}{m_\delta}\right)^{-m_\delta}\mathrm{d}z. \tag{48}$$

Unluckily, $\frac{\mathrm{d}^\upsilon}{\mathrm{d}s^\upsilon}h(e(s))$ in (46) is still in the form of composite function, which inevitably yields another application of Faà di Bruno's formula in the derivation later. The u-th derivative of $b(x)$ can be calculated as

$$b^{(u)}(s)=\frac{(m_{\mathrm{N}}+u-1)!}{(m_{\mathrm{N}}-1)!}\left(1+\frac{sP_{\mathrm{M}}\left(r^2+h_{\mathrm{M}}^2\right)^{-\frac{\alpha_{\mathrm{N}}}{2}}}{m_{\mathrm{N}}}\right)^{-m_{\mathrm{N}}-u}\left(-\frac{P_{\mathrm{M}}\left(r^2+h_{\mathrm{M}}^2\right)^{-\frac{\alpha_{\mathrm{N}}}{2}}}{m_{\mathrm{N}}}\right)^{u}, \tag{49}$$

while the high order derivative of $h(x)$ and $e(x)$ is respectively given by

$$h^{(\upsilon)}(s)=\begin{cases}\dfrac{N_{\mathrm{s}}!}{(N_{\mathrm{s}}-\upsilon)!}s^{N_{\mathrm{s}}-\upsilon}, & \upsilon\leq N_{\mathrm{s}},\\ 0, & \upsilon>N_{\mathrm{s}},\end{cases} \tag{50}$$

$$e^{(\eta)}(s)=\sum_{\delta\in\{\mathrm{L},\mathrm{N}\}}\frac{(m_\delta+\eta-1)!}{(m_\delta-1)!}\int_{\tilde{z}}^{z_{\mathrm{u}}}p_\delta(z)f_{Z_{i,n}}(z|r)\left(-\frac{P_{\mathrm{A}}z^{-\alpha_\delta}}{m_\delta}\right)^{\eta}\left(1+\frac{sP_{\mathrm{A}}z^{-\alpha_\delta}}{m_\delta}\right)^{-m_\delta-\eta}\mathrm{d}z. \tag{51}$$

Hence, by applying Faà di Bruno's formula over (46), we have

$$\begin{aligned}g^{(\tau)}(s)&=2\pi\lambda_{\mathrm{M}}\sum_{\upsilon=0}^{\tau}\binom{\tau}{\upsilon}\int_0^{\infty}b^{(\tau-\upsilon)}(s)\sum_{(k_1,\cdots,k_\upsilon)\in\mathcal{N}_\upsilon(N_{\mathrm{s}})}\frac{\upsilon!h^{(K_\upsilon)}(e(s))}{\prod_{\eta=1}^{\upsilon}k_\eta!}\prod_{\eta=1}^{\upsilon}\left(\frac{e^{(\eta)}(s)}{\eta!}\right)^{k_\eta}r\mathrm{d}r\\
&=2\pi\lambda_{\mathrm{M}}\sum_{\upsilon=0}^{\tau}\binom{\tau}{\upsilon}\sum_{(k_1,\cdots,k_\upsilon)\in\mathcal{N}_\upsilon(N_{\mathrm{s}})}\frac{\upsilon!}{\prod_{\eta=1}^{\upsilon}k_\eta!}\frac{N_{\mathrm{s}}!}{(N_{\mathrm{s}}-K_\upsilon)!}\int_0^{\infty}\frac{(m_{\mathrm{N}}+\tau-\upsilon-1)!}{(m_{\mathrm{N}}-1)!}\\
&\quad\times\left(1+\frac{sP_{\mathrm{M}}\left(r^2+h_{\mathrm{M}}^2\right)^{-\frac{\alpha_{\mathrm{N}}}{2}}}{m_{\mathrm{N}}}\right)^{-m_{\mathrm{N}}-\tau+\upsilon}\left(-\frac{P_{\mathrm{M}}\left(r^2+h_{\mathrm{M}}^2\right)^{-\frac{\alpha_{\mathrm{N}}}{2}}}{m_{\mathrm{N}}}\right)^{\tau-\upsilon}\\
&\quad\times\left(\sum_{\delta\in\{\mathrm{L},\mathrm{N}\}}\int_{\tilde{z}}^{z_{\mathrm{u}}}p_\delta(z)f_{Z_{i,n}}(z|r)\left(1+\frac{sP_{\mathrm{A}}z^{-\alpha_\delta}}{m_\delta}\right)^{-m_\delta}\mathrm{d}z\right)^{N_{\mathrm{s}}-K_\upsilon}\\
&\quad\times\prod_{\eta=1}^{\upsilon}\left(\sum_{\delta\in\{\mathrm{L},\mathrm{N}\}}\binom{m_\delta+\eta-1}{m_\delta-1}\int_{\tilde{z}}^{z_{\mathrm{u}}}\left(-\frac{P_{\mathrm{A}}z^{-\alpha_\delta}}{m_\delta}\right)^{\eta}\frac{p_\delta(z)f_{Z_{i,n}}(z|r)}{\left(1+\frac{sP_{\mathrm{A}}z^{-\alpha_\delta}}{m_\delta}\right)^{m_\delta+\eta}}\mathrm{d}z\right)^{k_\eta}r\mathrm{d}r.\end{aligned} \tag{52}$$

Finally, the expression of $\mathcal{L}_{I_{\Phi_+}}^{(\kappa)}(s)$ in (24) can be reached by plugging (52) into (45).

Appendix D
Proof of Theorem 1

The proof takes $\mathcal{O}_{\mathrm{M}}^{\mathrm{NC}}(x_0)$ as an example, for which the expression is given by

$$\begin{aligned}\mathcal{O}_{\mathrm{M}}^{\mathrm{NC}}(x_0)&=\mathbb{P}\left(\frac{\beta_{\mathrm{M}}V_1}{\mu\beta_{\mathrm{A}}I_{\mathrm{b}_0}+I_{\Psi_0}+I_{\Phi_+}}<\epsilon\right)=\mathbb{P}\left(V_1<\frac{\epsilon}{\beta_{\mathrm{M}}-\mu\beta_{\mathrm{A}}\epsilon}\left(I_{\Psi_0}+I_{\Phi_+}\right)\right)\\
&\overset{(a)}{=}1-\sum_{n=0}^{m_{\mathrm{N}}-1}\frac{\left(\xi_{\mathrm{M}}^{\mathrm{NC}}\left(I_{\Psi_0}+I_{\Phi_+}\right)\right)^n}{n!}\exp\left(-\xi_{\mathrm{M}}^{\mathrm{NC}}\left(I_{\Psi_0}+I_{\Phi_+}\right)\right)\\
&\overset{(b)}{=}1-\sum_{n=0}^{m_{\mathrm{N}}-1}\frac{\left(\xi_{\mathrm{M}}^{\mathrm{NC}}\right)^n}{n!}\sum_{(q_1,q_2)\in\mathcal{Q}_2(n)}\binom{n}{q_1,q_2}\\
&\quad\times\mathbb{E}\left[I_{\Psi_0}^{q_1}\exp\left(-\xi_{\mathrm{M}}^{\mathrm{NC}}I_{\Psi_0}\right)I_{\Phi_+}^{q_2}\exp\left(-\xi_{\mathrm{M}}^{\mathrm{NC}}I_{\Phi_+}\right)\right],\end{aligned} \tag{53}$$

where (a) follows from the CDF of Gamma distributed RV, and (b) follows from polynomial expansion. Since $\mathbb{E}_I\left[I^l \exp\left(-sI\right)\right] = (-1)^l \mathcal{L}_I^{(l)}(s)$, we can change the power of interference into the high order derivative of LT. Finally, by plugging in the expression of the LT and its high order derivative, we can reach the expression of $\mathcal{O}_{\mathrm{M}}^{\mathrm{NC}}(x_0)$ in (25).

The derivation of (26) and (27) follows similar procedure and is omitted due to space limit.

REFERENCES

[1] M. Giordani, M. Polese, M. Mezzavilla, *et al.*, "Toward 6G networks: Use cases and technologies," *IEEE Commun. Mag.*, vol. 58, no. 3, pp. 55–61, Mar. 2020.

[2] S. Chen, J. Zhang, E. Björnson, *et al.*, "Structured massive access for scalable cell-free massive MIMO systems," *IEEE J. Sel. Areas Commun.*, vol. 39, no. 4, pp. 1086–1100, Apr. 2021.

[3] S. Chen, J. Zhang, J. Zhang, *et al.*, "A survey on user-centric cell-free massive MIMO systems," *Dig. Commun. Netw.*, vol. 8, pp. 695–719, Dec. 2021.

[4] Y. Lu, B. Ai, Z. Zhong, *et al.*, "Energy-efficient task transfer in wireless computing power networks," *IEEE Internet Things J.*, vol. 10, no. 11, pp. 9353–9365, Jun. 2023.

[5] W. Sun, Z. Li, Q. Wang, *et al.*, "FedTAR: Task and resource-aware federated learning for wireless computing power networks," *IEEE Internet Things J.*, vol. 10, no. 5, pp. 4257–4270, Mar. 2023.

[6] D. Liu, Y. Xu, J. Wang, *et al.*, "Opportunistic UAV utilization in wireless networks: Motivations, applications, and challenges," *IEEE Commun. Mag.*, vol. 58, no. 5, pp. 62–68, May 2020.

[7] M. Mozaffari, X. Lin, and S. Hayes, "Toward 6G with connected sky: UAVs and beyond," *IEEE Commun. Mag.*, vol. 59, no. 12, pp. 74–80, Dec. 2021.

[8] H. Wu, Z. Wei, Y. Hou, *et al.*, "Cell-edge user offloading via flying UAV in non-uniform heterogeneous cellular networks," *IEEE Trans. Wireless Commun.*, vol. 19, no. 4, pp. 2411–2426, Apr. 2020.

[9] Y. Sun, Z. Ding, and X. Dai, "A user-centric cooperative scheme for UAV-assisted wireless networks in malfunction areas," *IEEE Trans. Commun.*, vol. 67, no. 12, pp. 8786–8800, Dec. 2019.

[10] X. Wang, H. Zhang, Y. Tian, *et al.*, "Modeling and analysis of aerial base station-assisted cellular networks in finite areas under LoS and NLoS propagation," *IEEE Trans. Wireless Commun.*, vol. 17, no. 10, pp. 6985–7000, Oct. 2018.

[11] J. Lee, Y. Kim, H. Lee, *et al.*, "Coordinated multipoint transmission and reception in LTE-advanced systems," *IEEE Commun. Mag.*, vol. 50, no. 11, pp. 44–50, Nov. 2012.

[12] Y. Yuan, S. Wang, Y. Wu, *et al.*, "NOMA for next-generation massive IoT: Performance potential and technology directions," *IEEE Commun. Mag.*, vol. 59, no. 7, pp. 115–121, Jul. 2021.

[13] M. Vaezi, R. Schober, Z. Ding, *et al.*, "Non-orthogonal multiple access: Common myths and critical questions," *IEEE Wireless Commun.*, vol. 26, no. 5, pp. 174–180, Oct. 2019.

[14] R. Ding, F. Gao, and X. S. Shen, "3D UAV trajectory design and frequency band allocation for energy-efficient and fair communication: A deep reinforcement learning approach," *IEEE Trans. Wireless Commun.*, vol. 19, no. 12, pp. 7796–7809, Dec. 2020.

[15] X. Huang, S. Leng, S. Maharjan, *et al.*, "Multi-agent deep reinforcement learning for computation offloading and interference coordination in small cell networks," *IEEE Trans. Veh. Technol.*, vol. 70, no. 9, pp. 9282–9293, Sep. 2021.

[16] J. Liu, M. Sheng, T. Q. S. Quek, *et al.*, "D2D enhanced co-ordinated multipoint in cloud radio access networks," *IEEE Trans. Wireless Commun.*, vol. 15, no. 6, pp. 4248–4262, Jun. 2016.

[17] L. Yang, T. J. Lim, J. Zhao, *et al.*, "Modeling and analysis of HetNets with interference management using Poisson cluster process," *IEEE Trans. Veh. Technol.*, vol. 70, no. 11, pp. 12 039–12 054, Nov. 2021.

[18] C. Skouroumounis, C. Psomas, and I. Krikidis, "A hybrid cooperation scheme for sub-6 GHz/mmWave cellular networks," *IEEE Commun. Lett.*, vol. 24, no. 7, pp. 1539–1543, Jul. 2020.

[19] W. Tang, H. Zhang, Y. He, *et al.*, "Performance analysis of multi-antenna UAV networks with 3D interference coordination," *IEEE Trans. Wireless Commun.*, vol. 21, no. 7, pp. 5145–5161, Jul. 2022.

[20] H. Zhang, M. Feng, K. Long, *et al.*, "Energy efficient resource management in SWIPT enabled heterogeneous networks with NOMA," *IEEE Trans. Wireless Commun.*, vol. 19, no. 2, pp. 835–845, Feb. 2020.

[21] A. Jee, K. Agrawal, and S. Prakriya, "A coordinated direct AF/DF relay-aided NOMA framework for low outage," *IEEE Trans. Commun.*, vol. 70, no. 3, pp. 1559–1579, Mar. 2022.

[22] A. Jee, K. Janghel, and S. Prakriya, "Performance of adaptive multi-user underlay NOMA transmission with simple user selection," *IEEE Trans. Cogn. Commun. Netw.*, vol. 8, no. 2, pp. 871–887, Jun. 2022.

[23] H. Zhang, H. Zhang, W. Liu, *et al.*, "Energy efficient user clustering, hybrid precoding and power optimization in Terahertz MIMO-NOMA systems," *IEEE J. Sel. Areas Commun.*, vol. 38, no. 9, pp. 2074–2085, Sep. 2020.

[24] M. Elhattab, M.-A. Arfaoui, and C. Assi, "CoMP transmission in downlink NOMA-based heterogeneous cloud radio access networks," *IEEE Trans. Commun.*, vol. 68, no. 12, pp. 7779–7794, Dec. 2020.

[25] X. Wang, H. Zhang, K. J. Kim, *et al.*, "Performance analysis of cooperative aerial base station-assisted networks with non-orthogonal multiple access," *IEEE Trans. Wireless Commun.*, vol. 18, no. 12, pp. 5983–5999, Dec. 2019.

[26] T. Hou, Y. Liu, Z. Song, *et al.*, "Multiple antenna aided NOMA in UAV networks: A stochastic geometry approach," *IEEE Trans. Commun.*, vol. 67, no. 2, pp. 1031–1044, Feb. 2019.

[27] H. Zhang, J. Zhang, and K. Long, "Energy efficiency optimization for NOMA UAV network with imperfect CSI," *IEEE J. Sel. Areas Commun.*, vol. 38, no. 12, pp. 2798–2809, Dec. 2020.

[28] X. Wang, H. Zhang, H. Yang, *et al.*, "On the performance of non-orthogonal transmission enabled two-tier CoMP networks," in *Proceedings of International Conference on Wireless Communications and Signal Processing (WCSP'2022)*, Nanjing, China, Nov. 2022, pp. 1–3.

[29] S. Chiu, D. Stoyan, W. Kendall, *et al.*, *Stochastic Geometry and its Applications*, 3rd ed. United Kingdom: John Wiley and Sons, 2013.

[30] A. Al-Hourani, S. Kandeepan, and S. Lardner, "Optimal LAP altitude for maximum coverage," *IEEE Wireless Commun. Lett.*, vol. 3, no. 6, pp. 569–572, Dec. 2014.

[31] G. Chen, L. Qiu, and C. Ren, "On the performance of cluster-based MIMO-NOMA in multi-cell dense networks," *IEEE Trans. Commun.*, vol. 68, no. 8, pp. 4773–4787, Aug. 2020.

[32] K. J. Kim, M. D. Renzo, H. Liu, *et al.*, "Performance analysis of distributed single carrier systems with distributed cyclic delay diversity," *IEEE Trans. Commun.*, vol. 65, no. 12, pp. 5514–5528, Dec. 2017.

[33] M. Ding and D. López-Pérez, "Performance impact of base station antenna heights in dense cellular networks," *IEEE Trans. Wireless Commun.*, vol. 16, no. 12, pp. 8147–8161, Dec. 2017.

[34] S. Singh, H. S. Dhillon, and J. G. Andrews, "Offloading in heterogeneous networks: Modeling, analysis, and design insights," *IEEE Trans. Wireless Commun.*, vol. 12, no. 5, pp. 2484–2497, May 2013.

[35] D. W. Matolak and R. Sun, "Air-ground channel characterization for unmanned aircraft systems - part III: The suburban and near-urban environments," *IEEE Trans. Veh. Technol.*, vol. 66, no. 8, pp. 6607–6618, Aug. 2017.